How will the dominant weather regimes change under the influence of climate warming?

Master's Thesis

M. Sc. Climate Physics:
Meteorology and Physical Oceanography

Christian-Albrechts-Universität zu Kiel
GEOMAR Helmholtz Centre for Ocean Research

submitted by:
Tabea Rahm
Matriculation Number: 1104231

Advisor: Prof. Dr. Joakim Kjellsson
Co-Advisor: Dr. Wenjuan Huo

Kiel, 18 April 2023

Abstract

Weather regimes are quasi-stationary and persistent atmospheric circulation patterns. They have been proven useful in describing the mid-latitude wintertime circulation and are commonly identified by applying a clustering algorithm to the mid-tropospheric geopotential height field. The four wintertime regimes that are typically recognised in the Euro-Atlantic sector are the positive and negative phases of the North Atlantic Oscillation (NAO), the Scandinavian Blocking, and the Atlantic Ridge regime. By impacting the large-scale atmospheric flow, the individual regimes have considerable influence on surface weather and extreme events. In this thesis, future atmospheric circulation changes in the Euro-Atlantic region are investigated within the weather regime framework. For this purpose, simulations performed by the Swedish Meteorological and Hydrological Institute's Large Ensemble (SMHI-LENS) with the global climate model EC-Earth3 are explored. The regime patterns arising from clustering geopotential height anomalies at the 500 hPa level are calculated for two ensemble simulations, one with historical and one with SSP5-8.5 scenario forcing, and compared to ERA5 reanalysis data. Firstly, four weather regimes are identified in the SMHI-LENS historical simulation. Three of these resemble the regimes identified in ERA5 and in previous studies reasonably well. Only the positive NAO phase is not captured by the ensemble. Under the strong global warming scenario in the SMHI-LENS, the regime patterns get weaker by the end of the century, with the exception of the NAO– regime, which experiences an enhancement of the geopotential height gradient. Composited near-surface temperature anomalies and extremes weaken, while precipitation anomalies and extremes intensify in response to global warming. The general patterns of the geopotential height, temperature, and precipitation anomaly composites, however, remain practically unchanged under the strong forcing scenario. The future changes in weather regimes simulated with the SMHI-LENS are seen to agree with the general shifts expected under global warming. Despite the disagreement between the observed and the simulated NAO+ regime, the SMHI-LENS as a single-model initial-condition large ensemble is shown to be a useful tool in robustly identifying independent circulation regimes and studying the accompanying surface weather conditions.

Table of Contents

List of Figures

List of Tables

List of Abbreviations

AA	Arctic amplification.
CMIP	Coupled Model Intercomparison Project.
DJF	December, January, February.
ECMWF	European Centre for Medium-Range Weather Forecasts.
ENSO	El Niño-Southern Oscillation.
EOF	Empirical orthogonal function.
ERA5	ECMWF reanalysis dataset covering 1979–present.
GCM	General circulation model.
IFS	Integrated Forecasting System.
IPCC	Intergovernmental Panel on Climate Change.
LSA	Linear sum assignment.
MJO	Madden-Julian Oscillation.
NAC	North Atlantic Current.
NAO	North Atlantic Oscillation.
PC	Principal Component.
RCP	Representative Concentration Pathway.
SAT	Near-surface air temperature.
ScenarioMIP	Scenario Model Intercomparison Project.
SMHI	Swedish Meteorological and Hydrological Institute.
SMHI-LENS	Swedish Meteorological and Hydrological Institute Large Ensemble.
SMILE	Single-model initial-condition large ensemble.
SSP	Shared Socioeconomic Pathway.
SST	Sea surface temperature.
WMO	World Meteorological Organization.
WR	Weather regime.
Z500	Geopotential height at 500 hPa.

1 Introduction

1.1 Motivation

According to the latest report of the Intergovernmental Panel on Climate Change (IPCC), the increase in global surface temperature for the decade 2011–2020 relative to pre-industrial conditions (1850–1900) is 1.09 [0.95 to 1.20] °C and human influence is the main driver of the rapidly changing climate (IPCC 2021: Arias et al. 2021). The expected consequences of climate change are manifold and far-reaching: Human health is endangered both directly and indirectly, inter alia by extreme weather events and the facilitated transmission of diseases due to the deterioration of environmental conditions (Kim et al. 2014). The economic impacts of climate warming are currently a highly debated research subject, but there is growing evidence that, in the long run, the negative impacts are likely to outweigh the positive ones (Tol 2018). Special challenges are also expected in the energy sector, which can be severely vulnerable to extreme weather events (Schaeffer et al. 2012). Last but not least, worst-case scenario models predict that almost one-third of the world's population will live in uninhabitable climatic conditions by the end of the century, which could lead to the migration of considerable parts of the human population in the future (Balsari et al. 2020).

Good knowledge of the possible range of future changes in weather and climate is vital for strategic approaches to mitigation and adaptation. Uncertainty in future projections, however, comes from the non-linear and chaotic nature of the weather system (Lorenz 1963) and the fact that the internal variability of the atmospheric circulation is typically large (Deser et al. 2012). Even if a perfect model existed and was forced by realistic external factors, predictions would still be sensitive to initial errors and reliable forecasts difficult on all scales (Ferranti et al. 2015). Large ensembles with a single model have been proven useful in distinguishing the response to external forcing from internal variability (Lehner et al. 2020; Deser et al. 2020).

One region known for its substantial natural variability is the North Atlantic (Deser et al. 2012). A suitable framework to study the internal modes of its atmospheric variability is to classify the large-scale circulation in terms of recurrent and persistent patterns that are mostly referred to as Weather regimes (WRs) (e.g. Michelangeli et al. 1995; Fabiano et al. 2020).

In this thesis, a large ensemble performed with the EC-Earth3 model is used to investigate the recurrent and persistent Euro-Atlantic WRs under a historical and a future scenario forcing. The remaining part of Section 1 introduces the concept of WRs and summarises current literature on expected changes under global warming. Section 2 describes the data and methods used to investigate changes in WRs. The results for WRs, associated temperature and precipitation changes, and extreme weather are described in Sections 3, 4, and 5, respectively. Section 6 discusses these findings before they are summarised to draw a conclusion in Section 7.

1.2 Concept and history of weather regimes

The atmospheric wintertime circulation in the Euro-Atlantic region is known to be very complex and highly variable. It is characterised by the chaotic nature of the weather system, shifts in the position of the jet stream, generation of persistent anticyclonic blockings (Barriopedro et al. 2006), and interaction with topography (Dorrington et al. 2022). Different approaches have been introduced to describe this variability. A powerful concept, derived from the 1940s idea of 'Großwetterlagen' (Baur et al. 1944; Levick 1949), which means general weather situations in German, is to classify the circulation in terms of WRs. The term 'Weather Regime' traces back to Rex (1951) and his description of the weather conditions accompanying European blocking.

In this WR framework, observed circulation variations (typically in geopotential height) are categorised into a limited number of recurrent, quasi-stationary patterns that persist longer than the usual life cycle of individual circulation disturbances (Reinhold and Pierrehumbert 1982; Hannachi et al. 2017). The Euro-Atlantic atmospheric wintertime circulation can then be described in terms of transitions between these WRs (Ferranti et al. 2015).

Mostly, four wintertime WRs are identified in the Euro-Atlantic sector (e.g. Michelangeli et al. 1995; Cassou 2008; Dawson et al. 2012; Ferranti et al. 2015; Fabiano et al. 2020). Following i.a. Fabiano et al. (2020), the four Euro-Atlantic regimes are:

- The positive phase of the North Atlantic Oscillation (NAO+), which shows a strong low-pressure anomaly south of Iceland and high pressure over southern latitudes. The NAO describes a large-scale atmospheric pressure see-saw identified as the leading mode of variability in the North Atlantic region (Hurrell et al. 2003).

- The Scandinavian Blocking pattern (sometimes also called European blocking, e.g. in Ferranti et al. (2015)), characterised by a strong high-pressure anomaly over the North Sea and western Scandinavia.

- The Atlantic Ridge pattern, showing high pressure over the middle of the North-Atlantic south of Iceland and Greenland and low pressure over northwestern Europe.

- The negative NAO phase (NAO–), which is characterised by a high-pressure anomaly over Greenland and lower pressure over southern latitudes.

The separation of the circulation into WRs can also be undertaken for the summer atmosphere (Cassou et al. 2005) or year-round (Vrac et al. 2014; Cortesi et al. 2021), although this mostly leads to different regime patterns. Identifying persistent WRs in spring and autumn is typically more difficult due to the higher variability of atmospheric circulation patterns during these seasons (Yiou et al. 2008).

The practical interest in the WR classification lies in the knowledge that the different WRs

influence the surface weather by impacting the large-scale atmospheric flow (Plaut and Simonnet 2001; Yiou and Nogaj 2004; Michel et al. 2012; Wiel et al. 2019), thereby affecting both mean and extreme events. In addition to the large-scale flow, local weather in the mid-latitudes is heavily influenced by the passage of cyclones that are related to precipitation, wind, and temperature extremes (Shaw et al. 2016). These extratropical cyclones aggregate in the Euro-Atlantic region along the North-Atlantic storm track and a relation between WRs and the location and orientation of the cyclone tracks has been described in previous studies (Pinto et al. 2009; Michel et al. 2012).

Each of the aforementioned wintertime WRs has very distinct impacts on the weather conditions over the Euro-Atlantic sector. The influence of the opposite phases of the NAO on the mean weather conditions has been identified in both observations and models: stronger surface westerlies during positive NAO phases favour wetter and warmer than normal weather over northern Europe and dry conditions over southern Europe and the Mediterranean region, while the weakening of the westerly winds during the negative phase is typically associated with anomalies of opposite sign (Hurrell et al. 2003; Pinto and Raible 2012). Scandinavian Blocking regimes were found to be connected to heat waves over Scandinavia and Iceland, but also cold spells over southeastern Europe due to the advection of polar air. In addition, a reduction in heavy precipitation over central Europe is frequently connected to this regime (Yiou and Nogaj 2004; Kautz et al. 2022). The presence of an Atlantic Ridge in the pressure field induces above-average temperatures and below-average precipitation in the region of the ridge as well as northwesterly winds over western and central Europe, although the responses in surface temperature and precipitation are generally weaker in the European region than for the other WRs (Plaut and Simonnet 2001; Wiel et al. 2019).

1.3 Weather regimes and climate change

Generally, changes in the mean climate are associated with changes in the frequency, intensity, location, duration, and timing of weather and climate extremes (IPCC 2021 technical summary: Arias et al. 2021) These shifts in extreme events can be linked to varying probability distributions of the respective variables as seen in the example of global surface temperature in Figure 1 (IPCC 2012). These possible changes in the shape and the mean of the probability distribution might mitigate but also reinforce each other, as displayed for cold and warm extremes, respectively, in Figure 1c.

Globally, an overall decrease in the number of cold days and nights and an increase in warm days and nights is observed along with a general intensification of the global water cycle that increased the severity of wet and dry extreme events (IPCC 2012 and 2021: Field et al. 2012; Arias et al. 2021).
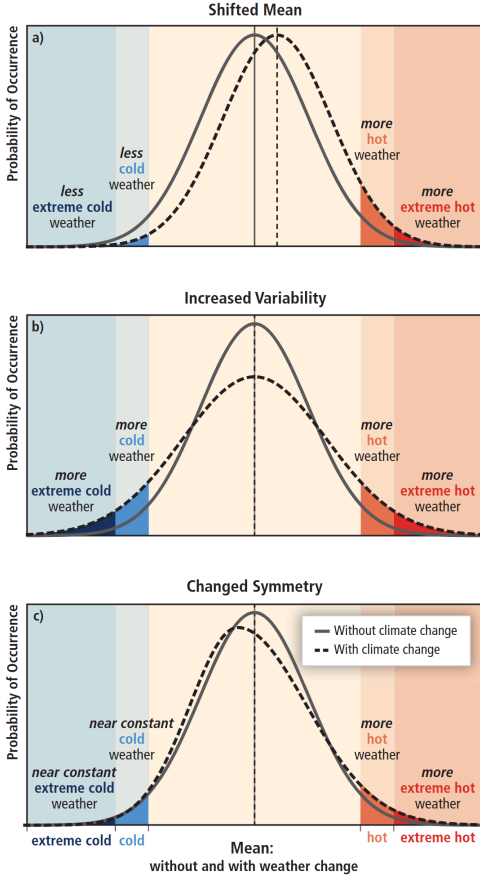
Figure 1: Possible shifts in the probability distribution of global surface temperature under the influence of climate change (IPCC 2012: Field et al. 2012).

Under a warming climate as simulated by current state climate models, a continuation of a positive trend in warm extreme frequency along with a decrease in the frequency of cold events is virtually certain, while an increase in the probability of heavy precipitation events for most locations is very likely (IPCC 2012 and 2021: Field et al. 2012; Arias et al. 2021). Naturally, regional differences are pronounced and deviations from this general trend are to be expected. Changes in the different atmospheric variables are interconnected, yet many cause-effect relationships still require further study. One of the most prominent connections is between temperature and precipitation. The ongoing and projected increase in atmospheric temperatures allows the atmospheric saturation vapour pressure to increase based on the Clausius-Clapeyron relation, which forms a thermodynamic constraint on precipitation given by an increase in precipitable water of 7% per degree of warming. It thereby affects both precipitation mean and extreme values in a changing climate (Field et al. 2012; Pendergrass et al. 2017), and, in general terms, precipitation appears to roughly follow the Clausius-Clapeyron relation. On a regional scale, however, precipitation observations and projections can significantly deviate from the increase expected from the Clausius-Clapeyron relation, e.g. in large parts of Europe and in the subtropics (Lenderink and van Meijgaard 2008; Pfahl et al. 2017). This indicates that other effects such as increased latent heat release and changes in atmospheric dynamics can allow for regional deviations. In fact, the current Coupled Model Intercomparison Project generation (CMIP6) still shows large uncertainties in extreme precipitation projections at the regional scale (John et al. 2022).

In an attempt to characterise future changes in mid-latitude circulation, the response of Euro-Atlantic WRs to global warming has also been explored in different modeling studies. An increase in NAO+ regime frequency was identified in both Hertig and Jacobeit (2014), by evaluating RCP8.5 scenario simulations with CMIP5 models, and Fabiano et al. (2021), by additionally including the current generation of CMIP models, i.e. CMIP6. Fabiano et al. (2021) also found the NAO+ regimes to be more persistent in different forcing scenarios. The

frequency of occurrence of the Scandinavian Blocking regime, on the other hand, was seen to decrease in their study (Fabiano et al. 2021), which is in contrast to a lack of significant changes in regime frequency and spatial patterns reported in Bacer et al. (2022). The latter authors used the WR approach to examine the impact of climate change on European blocking. The Atlantic Ridge regime's frequency was seen to increase in RCP8.5 simulations with CMIP5 models (Hertig and Jacobeit 2014), whereas a decrease in regime frequency was identified when also including CMIP6 models (Fabiano et al. 2021). For the negative NAO phase, a consistent increase in regime frequency was found in Cattiaux et al. (2013a) in the majority of CMIP5 models. However, Hertig and Jacobeit (2014), who evaluated CMIP5 ensembles, described the representation of the NAO− regime to be highly variable in the historical and scenario runs, suggesting that the regime is not represented correctly in the GCM simulations.

This short review of previous work on the effect of climate change on WR characteristics shows a substantial disagreement between the different studies. The common methodology used in these studies is to project the data from the future simulation onto the WRs identified in a reference dataset, mostly given by reanalysis data. This ensures the identification of the same regimes in the future simulation and allows the evaluation of changes in regime statistics (such as regime frequency and persistence). At the same time, this approach implies that the spatial structure of the regime patterns is time-invariant. Considering the possibly manifold changes in atmospheric circulation in response to different degrees of global warming, this assumption does not necessarily hold as changes in the spatial patterns or even the emergence of new WRs are conceivable. The projection of the future simulation onto historical WR patterns, however, cannot capture spatial changes or potentially new WRs (Ullmann et al. 2014; Dorrington et al. 2022).

In this thesis, the WRs are identified in regard to the respective climates rather than projecting the model data onto the regime patterns identified in a reference dataset. Thereby, no assumption about the spatial time-invariance of the regime patterns is made and we cannot, a priori, expect to find the known circulation regimes, but instead attempt to identify the circulation patterns in the Euro-Atlantic region that are inherent to the observed and simulated climates. In this context, using a large initial condition climate model ensemble allows the robust identification of the forced response of the regimes to a strong warming scenario for the historical and future periods independently.

2 Data and Methods

2.1 Data

This thesis makes use of reanalysis data and results from climate model ensemble simulations. For both, geopotential (height) at 500 hPa, near-surface air temperature (SAT), and total precipitation are retrieved from the respective sources.

2.1.1 The ERA5 reanalysis

Daily ERA5 reanalysis (Hersbach et al. 2020) data from the European Centre for Medium-Range Weather Forecasts (ECMWF) are used as an estimate of the atmospheric state for the historical period. ERA5 uses the Integrated Forecasting System (IFS) Cy41r2 to assimilate historical atmospheric observations (Hersbach et al. 2020). The dataset analysed in this thesis covers the period from 01.01.1979 to 31.12.2021, yielding 43 full years of reanalysis data. ERA5 data are available with a spatial resolution of approximately 0.25° horizontally and 37 pressure levels between 1000 to 1 hPa vertically. For this thesis, data interpolated by bi-linear interpolation onto an even spatial grid with a horizontal resolution of 1° x 1° is used.

2.1.2 The SMHI Large Ensemble with EC-Earth3

In addition, climate model ensemble projections are used to assess the impact of future climate change on WRs. The model ensemble at hand was created by the Swedish Meteorological and Hydrological Institute (SMHI). The SMHI performed a large ensemble of climate model simulations, the SMHI Large Ensemble (SMHI-LENS), using EC-Earth3 version 3.3.1 (Döscher et al. 2021).

2.1.2.1 EC-Earth3

EC-Earth3 is a non-operational global Earth system model developed and maintained by the European research consortium EC-Earth (Döscher et al. 2021), which is used as a contribution to the Coupled Model Intercomparison Project Phase 6 (CMIP6; Eyring et al. 2016). The atmospheric model, IFS Cy36r4, uses a time step of 45 min and the spectral truncation T255 in combination with a linearly reduced Gaussian grid at N128 resolution. There are 91 levels between the surface and 1 hPa in the vertical. This atmospheric model is coupled at every time step to the NEMO3.6 ocean model, which includes the sea ice model LIM3 (Wyser et al. 2021). The data have a daily temporal resolution, which is common for the computation of weather regimes as described in Section 2.2, and were remapped to an evenly spaced horizontal grid with a resolution of 2° x 2° to reduce the required memory capacity.

2.1.2.2 Ensemble experiments design

The SMHI-LENS is a single-model initial-condition large ensemble (SMILE). A SMILE represents the range of internal variability by running multiple simulations with the same climate model but applying slightly different initial conditions. This allows taking into account the role of internal variability when investigating the atmospheric response to climate change (Deser et al. 2012; Lehner et al. 2020; Maher et al. 2021; Mittermeier et al. 2022). The SMHI-LENS consists of 50 members, which cover the period 1970 – 2100, and features different Shared Socioeconomic Pathway (SSP) scenarios (Wyser et al. 2021). All simulations of a given SSP experiment are subject to identical external forcings following the CMIP6 and Scenario Model Intercomparison Project (ScenarioMIP) protocol (Jensen et al. 2022).

Out of these SSPs, SSP5-8.5 is the most extreme scenario and supersedes the predecessor Representative Concentration Pathway (RCP) 8.5 which was used in CMIP5. It assumes an energy-intensive, fossil-based economy. The greenhouse gas emissions in this scenario lead to a radiative forcing level of 8.5 Wm^{-2} in 2100, which corresponds to a strong warming signal in global mean near-surface temperature of around 6°C, relative to the years 1850–1900 as a baseline (O'Neill et al. 2016; Wyser et al. 2021).

For this thesis, two sets of ensembles are used, consisting of 50 members each: a historical simulation covering the period 01.01.1970–31.12.2014 and a future high emission SSP5-8.5 scenario simulation covering 01.01.2070–31.12.2100. The initial conditions of the different members of each ensemble were obtained by SMHI from branching off breeding simulations that were started from six members of the historical experiment for CMIP6. From running these six breeding simulations for 20 years each, 50 initial states were chosen for the atmosphere and the ocean and used as initial conditions for the large ensemble. Table 1 in Wyser et al. (2021) lists the model times at which the breeding experiments were branched off for the different ensemble members. The initial date for each member was set to 01.01.1970 (Wyser et al. 2021).

2.1.2.3 Data pretreatment

The calculation of weather regimes is based on the analysis of an atmospheric circulation variable, in this case geopotential height anomalies at the 500 hPa pressure level (Z500). Since the ERA5 reanalysis dataset only contains geopotential, it is converted to geopotential height by division by the value used by the World Meteorological Organization (WMO) for the Earth's gravitational acceleration of g=9.80665 ms^{-2}.

Total precipitation is provided in different units in the ERA5 reanalysis and the SMHI-LENS. In ERA5, precipitation is available in m per hour and is converted to mm/day by multiplying by a factor of 24000. The SMHI-LENS, however, provides precipitation in $kgm^{-2}s^{-1}$, which is converted to mm/day by multiplication with a factor of 86400.

In addition, the model ensemble members in this thesis are concatenated along the time dimension to obtain a longer time series of 50 times 30 years (= 1500 years) of data for both the historical and the future simulation. This could reduce the impact of noise by reliably covering the different modes of internal variability that are represented in the model (compare Strommen et al. 2019).

2.2 Methods

2.2.1 Calculation of weather regimes

1) Anomalies from the seasonal cycle

Following the steps described by Fabiano et al. (2020), the raw Z500 data is preprocessed to get boreal wintertime anomalies as input to the clustering algorithm used to determine the weather regimes.

The mean seasonal cycle is calculated by averaging over the given period by day of the year and then applying a 20-day running mean to average out higher frequency variations caused by internal variability. Anomalies are computed by subtracting the daily climatology, which is taken over different periods for the different data sets: 1979–2021 for ERA5, 1980–2010 for the historical simulations and 2070–2100 for the SSP5-8.5 projections.

In the next step, this seasonal cycle is subtracted from the daily Z500 data to obtain a time series of daily geopotential height anomalies from the seasonal cycle.

Following Fabiano et al. (2020), no detrending was applied to the data in the final analysis, since the trend in Z500 was found to be of the same order as decadal variability for some regions. Also, sensitivity tests in the early stage of this thesis showed that the resulting weather regimes are insensitive to detrending.

2) Clustering

In this thesis, the k-means clustering algorithm is used to identify atmospheric circulation regimes (MacQueen 1967; Lloyd 1982). The term "k-means" was first introduced by MacQueen (1967). This algorithm is an unsupervised partitional clustering approach, meaning that the dataset is decomposed into a set of k disjoint clusters. In an iterative process, each data point in the given dataset is assigned to the nearest cluster centroid. The nearest centroid is found using the Euclidean metric as a measure of distance. The number of clusters has to be chosen by the data analyst and various studies describe different approaches to selecting the right number of clusters (e.g. Chiang and Mirkin (2007) tested different methods). For this thesis, the number of clusters is given by the number of Euro-Atlantic WRs, which is mostly reported to be four (see Section 1 Introduction).

After the data analyst has decided on the number k of clusters, the general algorithm can be summarised in four steps (Arthur and Vassilvitskii 2006; Ikotun et al. 2023), that aim to maximise the variance between the clusters while at the same time minimising the variance within a given cluster. The steps are:

1. Randomly assign k objects from the given dataset as initial cluster centroids.

2. Assign each object in the dataset to the closest cluster centroid.

3. After assigning all objects, calculate the new positions of the cluster centroids.

4. Repeat steps 2 and 3 until nothing changes anymore, indicating that the algorithm has found a minimum.

The k-means clustering algorithm is non-deterministic, which means that the outcome of applying the algorithm can differ between runs. This is mostly due to the initialisation of the clusters which requires a random initial seed. If the system has multiple local minima, the algorithm can result in different clusters, depending on the initial seeds. Hence, a careful selection of these initial seeds needs to be made as described in Arthur and Vassilvitskii (2006). Following their report, the k-means++ method is applied to choose the initial states. To ensure that the clusters found by the algorithm are stable, the above steps were repeated with different random initial seeds and the regime patterns were found to be robust for all datasets.

To identify the dominant WRs, this clustering algorithm is applied to a low-dimensional truncated phase space. The phase space is obtained by applying empirical orthogonal function EOF analysis to a circulation variable, here boreal wintertime (December, January, and February: DJF) Z500 anomalies weighted by the cosine of latitude to account for different grid box sizes. Following i.a. Fabiano et al. (2020), the phase space spanned by the leading four EOFs is used. These explain more than 50% of the variance for all datasets as can be seen in Table A1 in the appendix. The exact region that is used for the definition of Euro-Atlantic WRs differs slightly in previous studies (e.g. in Cassou (2008), Cattiaux et al. (2013b), Wiel et al. (2019), and Bacer et al. (2022)). In this thesis, a latitude range of 30 °N to 90 °N and a longitude band covering 80 °W to 40 °E are used, which agrees with the Euro-Atlantic region used in various earlier studies (Dawson et al. 2012; Ferranti et al. 2015; Madonna et al. 2017; Strommen et al. 2019; Fabiano et al. 2020; Dorrington and Strommen 2020).

3) Regime frequencies

For each weather regime, the frequency of occurrence is calculated as the ratio of days within this certain regime to the total number of days in the given dataset. For the historical and the future simulations performed with the SMHI, the regime frequencies are calculated after concatenating the ensemble members along the time dimension as described above.

4) Compositing

Maps of the anomalies related to the different WRs are obtained by taking the mean across all daily fields that are assigned by the clustering algorithm to a given regime. The compositing is performed for wintertime Z500, near-surface air temperature (SAT), and total precipitation anomalies from climatology.

5) Regime attribution

The order of the labels found by the k-means clustering algorithm is arbitrary. Many studies have identified regime patterns in reanalysis data before, so the attribution for the WRs in ERA5 was possible to be performed 'by eye', i.e. by subjectively comparing the patterns to the literature.

To objectively identify the pairs of the SMHI-LENS historical regimes and WRs in ERA5 that agree best, the linear sum assignment (LSA) method (Dorrington et al. 2022) was applied, since this technique aims to minimise a cost matrix. In our case, the cost matrix equals the correlation matrix between the different clusters. More precisely, the correlation matrix is given by the area-weighted pattern correlations of all possible combinations between the regime patterns identified in ERA5 and in the SMHI-LENS historical simulation. Since the LSA algorithm aims to solve a minimising task but we seek the combination that maximises the correlation between the two datasets, the correlation matrix with inverted sign is used as the cost matrix.

6) Robustness testing

After compositing the geopotential height anomalies, the robustness of the anomalies found for each weather regime is tested. For each grid point, the fraction of days that agree on the sign of the composited anomaly is calculated. If at least 80% of the days show the same sign, the composited anomaly at that grid point is considered to be robust.

2.2.2 Extreme weather

The definition of extreme weather (e.g. extreme temperature or precipitation) is always somewhat arbitrary since a threshold has to be defined beyond which anomalies are counted as 'extreme weather' (Walsh et al. 2020). This threshold can be a concrete value taken from the distribution (e.g. defining temperatures at or below -50°C at the South Pole as extreme cold events (Keller et al. 2022)), or a value relative to the distribution (e.g. 1.5 standard deviations or the 99th percentile (Wheeler et al. 2011; Pendergrass et al. 2016)).

A commonly used range is given by the 5th to 95th percentile (e.g. IPCC 2021: Arias et al. 2021). In this framework, the values below the 5th percentile are considered 'low extremes' while the values above the 95th percentile are counted as 'high extremes'. In the case of temperatures, this corresponds to cold and warm extremes. According to Coelho et al. (2008) and Heikkilä

et al. (2011), the thresholds given by the 5$^{\text{th}}$ and the 95$^{\text{th}}$ percentile, respectively, represent a good compromise between a cutoff value that is high enough to define extreme weather events and a sufficient occurrence of exceedances of the threshold to represent those events.

SAT and precipitation anomalies corresponding to the 5$^{\text{th}}$ and 95$^{\text{th}}$ percentiles in the historical simulation are used as thresholds for the anomalies in the SSP5-8.5 scenario simulation to show the spatial changes in the distribution of anomalies under global warming, as described next.

Firstly, SAT and total precipitation anomalies from the seasonal cycle are calculated, separately for the historical (1980–2010) and the future periods (2070–2100).
Secondly, the time series of anomalies are composited into the different WRs, based on the labels obtained from clustering the respective geopotential height.
In the next step, the 5$^{\text{th}}$ and the 95$^{\text{th}}$ percentile are computed for the different WRs at each grid point from the historical simulation time series to serve as thresholds for low and high extremes. This way, the threshold is determined by the distribution of the (simulated) present-day climate at each grid point individually, hence taking into account geographical differences in variability.
Finally, these thresholds as obtained from the historical simulation are used to estimate the future probability of extreme events with a comparable magnitude as in the (simulated) present-day climate for every grid point. An example: if the temperature anomaly that corresponds to the 5$^{\text{th}}$ percentile in a certain regime in the historical simulation (e.g. -4 K at a certain latitude and longitude) is projected to occur in less than 5% of the days within this same future regime, it can be said that cold extremes with the same magnitude as in the present-day climate are expected to occur less frequently or to become less extreme at this grid point.

2.2.3 Storm tracks

Following early studies in the 1970s and 1980s as well as more recent publications, storm tracks can be identified as regions of increased high-frequency fluctuations in the geopotential height field (Sawyer 1970; Blackmon 1976; Lau 1988; Trigo 2006; Chu et al. 2013; Yang et al. 2021).

Hence, the North-Atlantic storm tracks and their activity are in the following represented by the standard deviation of six-day high-pass filtered wintertime (DJF) Z500. The six-day high-pass filtering was performed by subtracting a six-day rolling mean from the raw Z500 data.

Different time filterings have been applied in various previous studies to extract the high-frequency fluctuations in geopotential height (see e.g. Lau 1988; Trigo et al. 2000; Sickmöller et al. 2000; Trigo 2006). For the purpose of this thesis, neglectable differences were seen when applying ten-day high-pass or band-pass filters (typically 2.5–6 days), and the method was set to a high-pass filter with six days as in Kidson and Sinclair (1995).

3 Weather regime patterns in present-day and future climate

To shed some light on the projected changes in WRs under a strong climate warming scenario as simulated by the SMHI-LENS, the following section first looks at the WR patterns that are calculated from the ERA5 reanalysis data and then compares them with the WRs in the historical and the SSP5-8.5 scenario simulation.

3.1 Historical weather regimes in the ERA5 reanalysis

The WR patterns identified in the ERA5 reanalysis by averaging over the daily Z500 anomaly fields assigned to the different clusters are shown in Figure 2.

The first and the last cluster (Fig. 2a and d) are consistent with the spatial patterns observed during the opposite phases of the North Atlantic Oscillation (NAO) (e.g. Hurrell et al. 2003) and referred to as NAO+ and NAO–, respectively. They are defined by a pronounced meridional gradient in Z500 anomalies caused by a robust trough over the North Atlantic (for NAO+), or a distinct ridge centred over the Labrador Sea (in the case of NAO–), and anomalies of opposite sign further south. The second WR (Fig. 2b) is identified as the Scandinavian Blocking regime as it is characterised by a large ridge over Scandinavia that is encircled by weaker negative anomalies. Finally, the remaining cluster (Fig. 2c) is referred to as the Atlantic Ridge regime and consists of a robust ridge over the North Atlantic and a negative Z500 anomaly over central and northern Europe.

Out of the four WRs identified in the ERA5 reanalysis, the Scandinavian Blocking regime appears most frequently with a regime frequency of 28.9% for the period 1979–2021. The NAO– regime, however, is the least frequent regime with 20.3%. NAO+ and Atlantic Ridge dominate the atmospheric circulation in 26.5% and 24.3% of the reanalysis days, respectively.

The WRs identified in ERA5 agree well with the regime patterns seen in many previous studies (e.g. Dawson et al. 2012; Ferranti et al. 2015; Strommen et al. 2019). Since the methodology in Fabiano et al. (2020) was followed closely to obtain the clusters for this thesis, the agreement with their study was expected and aimed for. Slight differences, e.g. in the shape of the trough(s) during the NAO– regime, can be due to their use of a different reanalysis product covering a different time period: Fabiano et al. (2020) computed WR patterns from a combination of the two ECMWF reanalyses ERA40 and ERA-Interim for the period 1957–2014.

The regime patterns identified in this thesis using the leading four EOFs for the clustering algorithm are relatively insensitive to the exact number of leading EOFs used in the clustering algorithm (see Figures A1 and A2 in the appendix). Also, in previous studies the regimes were
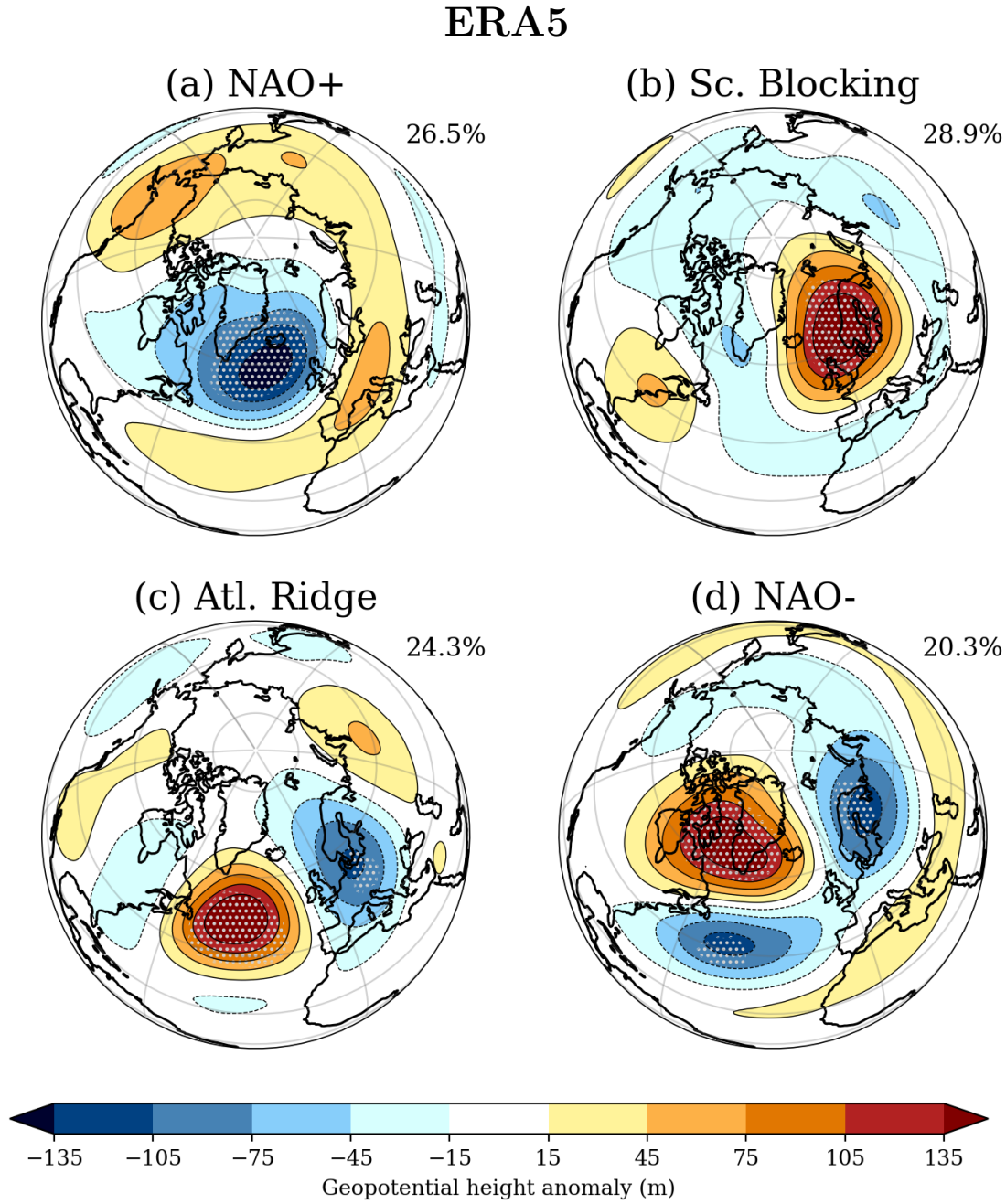
Figure 2: Composited geopotential height anomalies for the weather regimes identified in ERA5 using the full time period 1979–2021. Grey hatching indicates robust anomalies at an 80% level. The percentage values next to the regime patterns show the frequency with which the respective weather regime occurred within the entire time period.

seen to be robust regardless of the number of leading EOFs used for clustering (Ferranti et al. 2015; Wiel et al. 2019) or the use of different reanalysis products (Cassou 2008; Cattiaux et al. 2013b; Delgado-Torres et al. 2022).

3.2 Historical weather regimes in the SMHI Large Ensemble

The WR patterns identified in the reanalysis dataset are taken as a reference to assess how well the climate model ensemble reproduces the WRs for the current climate. The regime patterns in the SMHI-LENS as composites of geopotential height anomalies for the historical period 1980–2010 are shown in Figure 3.

To start with the cluster that visually agrees most with its observational counterpart, the Scandinavian Blocking regime (Fig. 3b) confidently reproduces the characteristic ridge over Scandinavia and the accompanying weaker negative anomalies. Also the robust ridge over the North Atlantic during the Atlantic Ridge regime (Fig. 3c) assorts well with the respective ERA5 cluster (Fig. 2c). The accompanying European trough, however, is stronger and located further south than in the reanalysis dataset, thereby squeezing the ridge and reducing its area. The NAO– cluster (Fig. 3d) still shows some accordance in the form of a negative Z500 anomaly over the North Atlantic albeit nearly completely missing the strong ridge that is centred over the Labrador Sea in ERA5 and the characteristic meridional gradient, which is much less pronounced in the SMHI-LENS. For the NAO+ regime (Fig. 3a), the features obtained from the SMHI-LENS historical simulation are not observed in the ERA5 reanalysis and the pattern more closely resembles the Atlantic Ridge regime in ERA5 (Fig. 2c) with a ridge located over the (eastern) North Atlantic and a trough in Z500 over Northern Europe.

It is worth pointing out that the method to identify the simulated WRs used here differs from Fabiano et al. (2020). They applied clustering to pseudo Principal Components obtained by projecting the simulated geopotential height fields onto the observational EOFs. Since the aim of this thesis is to investigate the WRs in future climates, the simulated regime patterns are identified independently from the reanalysis data not to have present-day EOFs as a reference.

Differences between observed and modelled WRs are visible for all regimes but by far most pronounced for the NAO+ regime. One can speculate that the smaller differences for the other patterns accumulate, in a sense, and that, since the clustering algorithm has to assign a fourth cluster, the NAO+ pattern is a remainder of the algorithm rather than the actual observed WR. To make the labelling consistent with the observed regimes, this regime will continue being referred to as the NAO+ regime in the SMHI-LENS, regardless of the assignment inconsistencies. One must keep in mind, however, that this regime pattern lacks any visual agreement with the observed NAO+ regime.

The regime frequencies for NAO+, Scandinavian Blocking, and NAO– have almost identical values, just over 25%, while the Atlantic Ridge regime occurs slightly less often, with a frequency of 23.7% in the historical ensemble simulations. This means that compared to the WRs in ERA5, the frequency of the NAO– regime is increased by ca. 5%, while the other regimes are to some extent under-represented in terms of their frequency of occurrence. Döscher et

Historical SMHI-LENS
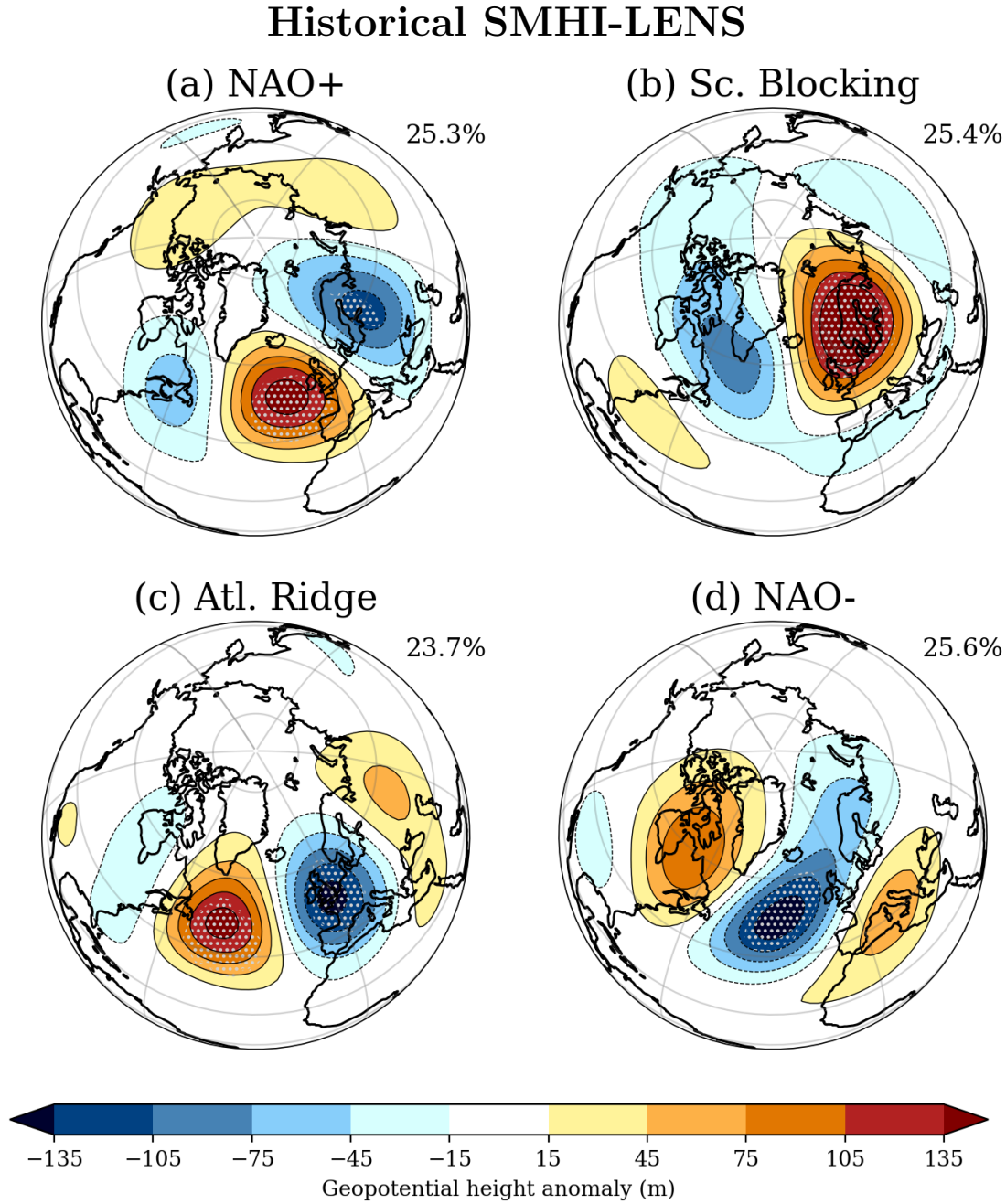
Figure 3: Composited geopotential height anomalies as in Figure 2 but for the weather regimes identified using the SMHI-LENS historical simulation covering the time period 1980–2010. Again, grey hatching indicates robust anomalies at an 80% level and regime frequencies are printed next to the regime patterns.

al. (2021) found that the common underestimation of winter European blocking in climate models is also present in EC-Earth3, which agrees well with the seen shortfall in Scandinavian Blocking regime frequency of three percentage points. However, this finding has to be treated with caution because of the significant differences in the simulated regime patterns compared to ERA5 since a changed spatial pattern will definitely impact the number of days assigned to this

SSP5-8.5 SMHI-LENS

(a) NAO+ 26.1%

(b) Sc. Blocking 24.5%

(c) Atl. Ridge 24.9%

(d) NAO- 24.4%

Geopotential height anomaly (m)

−135 −105 −75 −45 −15 15 45 75 105 135
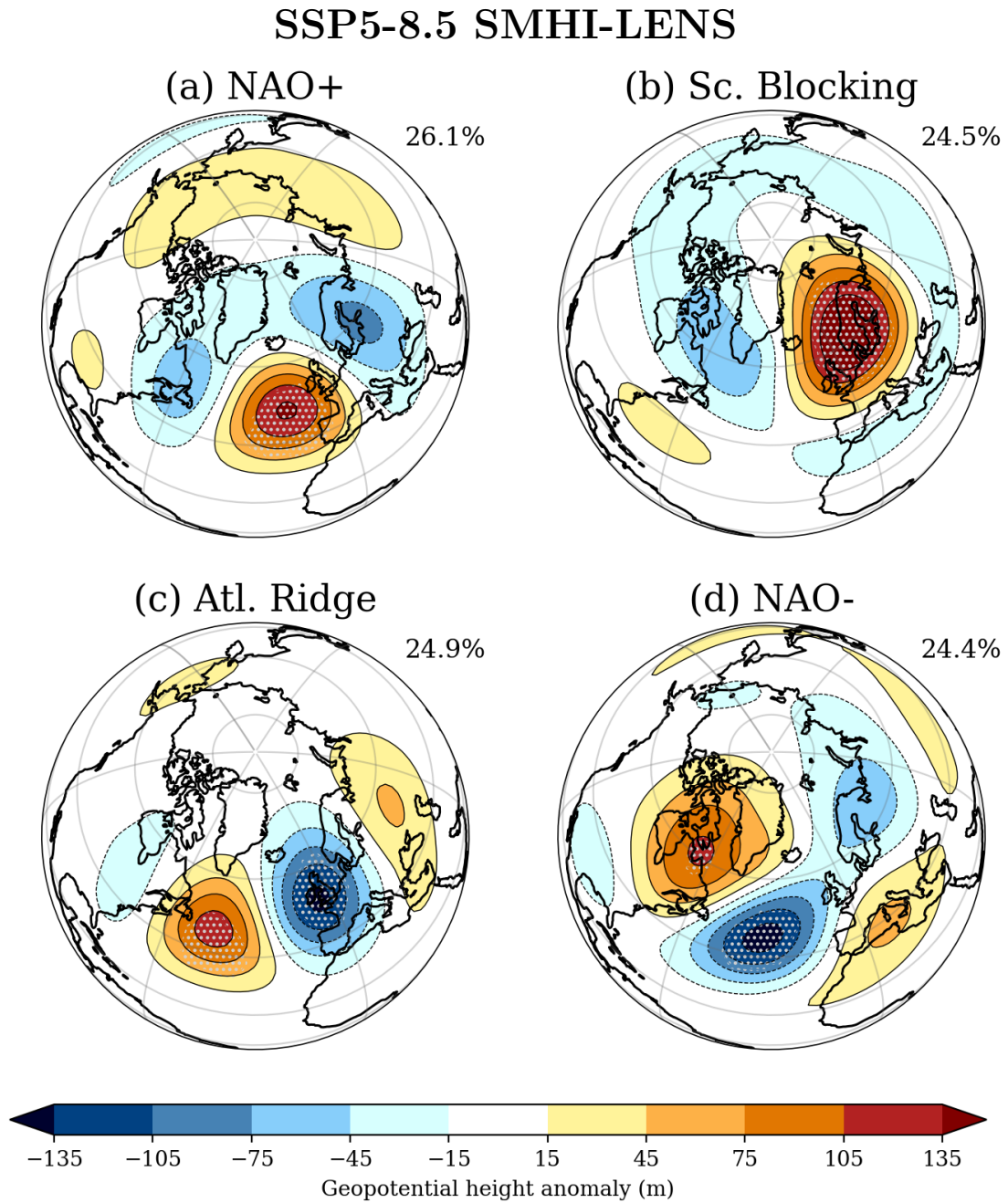
Figure 4: Composited geopotential height anomalies as in Figure 2 but for the weather regimes identified in the SMHI-LENS future simulation for the time period 2070–2100. Again, grey hatching indicates robust anomalies at an 80% level and regime frequencies are printed next to the regime patterns.

specific cluster but thereby also to the other regime frequencies. This means that although the Scandinavian Blocking regime pattern is reproduced fairly well by the model, the differences in the other regimes will definitely affect this regime and its frequency of occurrence.

The upper row of Table A2 lists spatial pattern correlation coefficients for the corresponding WR patterns identified in the historical simulation and in ERA5. These correlation coefficients

confirm that the Scandinavian Blocking regime in the SMHI-LENS historical simulation looks most like its reanalysis counterpart, while Atlantic Ridge and NAO– still resemble the regimes in the ERA5 reanalysis. The NAO+ regime, however, does not agree with the reanalysis dataset and even has a slightly negative pattern correlation coefficient.

3.3 Future weather regimes in the SMHI Large Ensemble

In the SMHI-LENS SSP5-8.5 scenario simulation for the end of the century, the general position of the Z500 anomalies for the different WRs in Figure 4 is very similar to the patterns in the historical simulation described in the previous section.

For the NAO+ regime pattern (Fig. 4a), both the ridge over the North Atlantic and the trough over northern Europe remain in place but decrease in magnitude compared to the historical ensemble. Future Scandinavian Blocking regimes (Fig. 4b) are projected to feature a strong ridge over Scandinavia that stays similar in magnitude. The surrounding trough gets less deep over the Labrador Sea. The Atlantic Ridge regime's positive Z500 anomaly (Fig. 4c) is still robustly located over the western North Atlantic at the end of the century but does not reach the same magnitude as in the historical ensemble simulation. The European trough associated with the Atlantic Ridge regime maintains a similar strength under the SSP5-8.5 scenario. During the NAO– regime (Fig. 4d), stronger positive anomalies over northeastern Canada are projected to stretch further over the Labrador Sea and Greenland, while a weak trough spreads further over northern Siberia. For all of the regimes under the SSP5-8.5 simulation, anomalies tend to not reach the same magnitude as in the historical simulation. Only the NAO– pattern exhibits a strengthening of the ridge over the Labrador Sea.

Regime frequencies only experience minor changes under the future scenario. By the end of the century, the NAO+ regime's frequency of occurrence is projected to increase to 26.1%. Also the Atlantic Ridge regime occurs more frequently than in the historical simulation with 24.9%, while both the Scandinavian Blocking and the NAO– regime dominate the tropospheric circulation less frequently than before with 24.5% and 24.4%, respectively.

The pattern correlation coefficients in the bottom row of Table A2 confirm the visual similarity between the patterns identified in the historical and the future scenario simulation with the lowest correlation coefficient being 0.9 for the NAO– regime. All the other WRs have a correlation above 0.92 and in line with the observation, the Scandinavian Blocking regime reaches the highest coefficient of 0.987.

Overall, the SMHI-LENS appears capable of producing four WRs, three of which are identified as the observed regimes. Under a future high-emission scenario, the associated geopotential height anomalies mostly experience a reduction in magnitude and only minor spatial changes.

4 Near-surface temperature and total precipitation patterns in present-day and future climate

4.1 Representation of and changes in simulated mean climate

To reliably simulate the future climate, a model ensemble first of all needs to be able to adequately represent the historical climate. The left column of Figure 5 illustrates this by showing the bias in mean climate in the SMHI-LENS (represented by SAT in Fig. 5a and total precipitation in Fig. 5c) compared to ERA5 reanalysis data for the historical period 1979–2014.

Near-surface temperatures in Figure 5a are generally too cold in the SMHI-LENS compared to ERA5 for the entire Arctic Ocean, most of the North Atlantic Ocean, Northern Europe, and Africa as well as most of the United States. The strongest cold bias can be seen in the Greenland and the Labrador Sea with SAT differences of below -6 K. Canada, East Siberia, and the Bering Sea, however, are on average warmer in the simulations than in the observations.

A cold bias in the western North Atlantic is a common feature of CMIP models with a spatial resolution of around 1° and it is also present in EC-Earth3 and the SMHI-LENS. This is often attributed to the misrepresentation of the path of the North Atlantic Current (NAC) at these resolutions: Compared to observations, the NAC direction is often shown as too zonal (Danabasoglu et al. 2014; Roberts et al. 2019). Meanwhile, Döscher et al. (2021) named the overestimation of winter sea ice concentration and thickness in the Arctic, and especially in the Labrador, the Greenland-Iceland-Norwegian, and the Barents Seas, as a reason for the cold bias. Sea ice concentration and thickness in the Bering Sea are, on the other hand, underestimated by EC-Earth3 (Döscher et al. 2021), which agrees well with the warm bias seen in this region.

The representation of total precipitation in the historical SMHI-LENS simulation (Fig. 5c) is characterised by a strong dry bias exceeding -1.5 mm/day over a region from the Labrador Sea southeastwards to the middle of the North Atlantic Ocean. Also most of the Arctic Ocean, northern Africa, and Eurasia are on average drier in the ensemble than in observations. Total precipitation is too high in the simulated historical climate along the North American coast and between the British Isles and Iceland.

These SAT and precipitation biases for the SMHI-LENS agree with the biases identified in Döscher et al. (2021) for EC-Earth3 in comparison to ERA5 (see their Figures 5b and 6b). When compared, the biases in SAT and precipitation show a clear connection: regions that show a cold bias are mostly characterised by a climate that is on average too dry in the ensemble simulations.
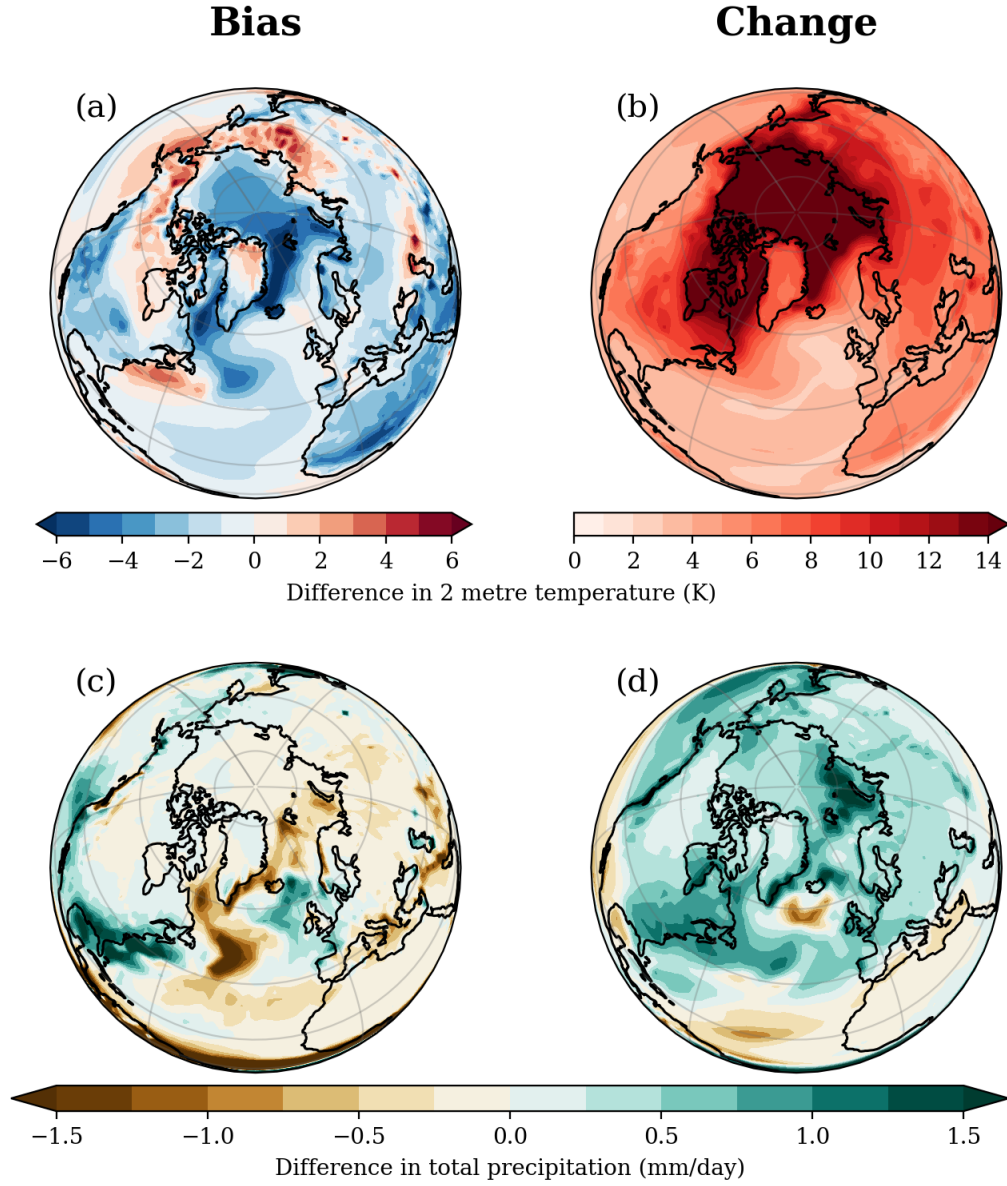
Bias

Change

Figure 5: Biases and future changes in the mean DJF climate simulated by the SMHI-LENS. Panels (a) and (c) show the bias between the historical simulation in the SMHI-LENS and the observational ERA5 reanalysis data for the period 1979–2014 for 2 metre temperature and total precipitation, respectively. For every grid point, the bias was obtained by subtracting the DJF mean in the reanalysis product from the DJF mean in the ensemble simulation data. Panels (b) and (d) display the changes in mean climate simulated by the SMHI-LENS following the SSP5-8.5 scenario compared to the historical simulation.

The right column in Figure 5 shows the simulated future changes in mean DJF SAT (Fig. 5b) and total precipitation (Fig. 5d). Positive values for the change indicate an increase in the respective variable for the future ensemble simulation compared to the historical simulation, whereas negative values correspond to a decrease.

Near-surface temperatures in Figure 5b increase towards a warmer climate everywhere in the Northern Hemisphere. The strongest warming happens over the Arctic region with differences to the simulated temperatures for the current climate of over +14 K. The weakest warming is seen in the North Atlantic south of 60 °N and lies in the range of +2–3 K. More than likely, the strong polar warming, especially over the Arctic Ocean, is a result of sea-ice loss, which in turn is caused by the generalised climate warming. Under the high-emission SSP5-8.5 scenario, even winter sea ice disappears (Wyser et al. 2021), yielding strong differences in DJF SAT since the future Arctic sea surface temperatures are generally much higher than the surface temperatures of sea ice and snow. The associated Arctic amplification (AA) of climate change in the high latitudes further enhances this difference in warming between high and lower latitudes (Wyser et al. 2021; Previdi et al. 2021).

Total precipitation in Figure 5d shows an increase at the end of the century under the SSP5-8.5 scenario for most of the regions north of 60 °N with the strongest increase of over +1.5 mm/day over the Kara and the Barents Sea. On northerly latitudes, only the region just south of Iceland gets drier in the future simulation. The Atlantic Ocean south of 60 °N as well as the northern part of the African continent tends to get drier in the future scenario compared to the historical simulation. Also the Mediterranean Sea gets drier under the SSP5-8.5 scenario.

Already Held and Soden (2006) have shown a tendency of wet-gets-wetter and dry-gets-drier in climate change experiments with coupled climate models, which agrees with the general observation of a wetting trend in the mid-latitudes and a drying of the subtropical regions in the SMHI-LENS future simulation. Although the wintertime precipitation reduction in the Mediterranean region has been reported in previous studies, the amplitude of the projected changes differs between different climate model simulations (Zappa et al. 2015). An Arctic wetting trend has been identified in many climate change projections before and current CMIP6 projections reveal even higher increases in Arctic precipitation than earlier simulations (see McCrystall et al. 2021, and references therein). The Kara and the Barents Seas are the regions pointed out by Wyser et al. (2021) to experience the strongest warming in the SMHI-LENS and to show clear AA. This strongly suggests that the strong precipitation increase is connected to an increase in AA.

A large proportion of the precipitation in the mid-latitudes is brought by extratropical cyclones, which aggregate in the Euro-Atlantic region along the North-Atlantic storm tracks as described in the introduction. For this thesis, storm tracks are identified as regions of enhanced standard deviation of six-day high-pass filtered Z500 anomalies (see Methods Section 2.2.3) and shown for the historical and the future scenario simulation in Figure 6.

(a) Historical   **(b) SSP5-8.5**

(c) Change
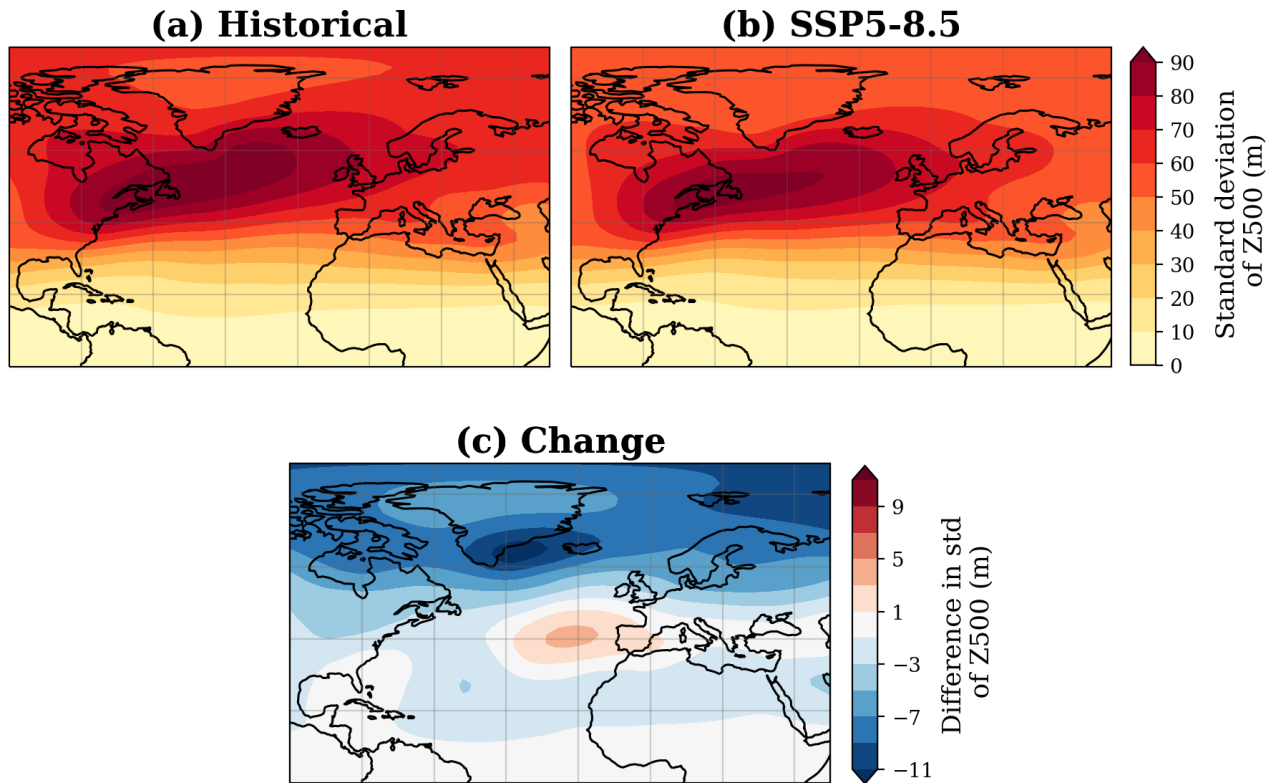
Figure 6: Storm tracks as seen in the standard deviation of wintertime six-day high-pass filtered Z500 anomalies in the SMHI-LENS (a) historical (1980–2010) and (b) future SSP5-8.5 (2070–2100) simulations. Panel (c) displays the difference between the future scenario minus the historical simulation.

In the historical simulation (Fig. 6a), storm tracks are most active in the area between Eastern Canada across the North Atlantic towards Europe. Peak values above 90 m in Z500 standard deviation are seen along a band reaching from Newfoundland to Iceland. This band is slightly tilted northeastwards towards the Denmark Strait.

According to the SSP5-8.5 scenario simulation (Fig 6b), the storm tracks are projected to maintain their general shape while weakening in most regions. Storm track activity as represented by Z500 standard deviation still reaches peak values of over 90 m, but the region is spatially more limited to a band off the coast of Newfoundland. Also, the southwest-northeast tilt of the storm tracks towards the Denmark Strait appears less pronounced under the SSP5-8.5 scenario with storm track activity rather following a more zonal track.

The change between the future and the historical simulation in Figure 6c confirms these observations. Generally, storm track activity gets weaker as seen in the dominating negative differences. The positive change in Z500 standard deviation off the coast of Spain, however, supports that the storm tracks in the SMHI-LENS are projected to become more zonal.

Generally within general circulation models GCMs, there is a tendency to produce North Atlantic storm tracks that are too zonally orientated (Zappa et al. 2013a; Catto et al. 2019), although a significant systematic improvement in the representation of the North Atlantic storm track was identified for the current CMIP6 models (Harvey et al. 2020).

Using the root mean square of band-pass filtered mean sea level pressure as a metric for storm tracks, similar patterns for the response to climate change have been identified by Harvey et al. (2020) for the CMIP6 multimodel average. Under the SSP2-4.5 scenario, a weakening of the northern flank of the North Atlantic storm track is accompanied by a modest zonal extension towards Europe. Also a reduction in the intensity of northern hemisphere extratropical cyclones in response to increasing atmospheric greenhouse gas concentrations was identified for CMIP5 models (Catto et al. 2019). Again, this agrees with the general decrease in storm track activity seen in Figure 6.

4.2 Observed influence of weather regimes on temperature and precipitation patterns

Applying regime compositing to ERA5 SAT and total precipitation anomalies yields the patterns shown in Figures 7 and 8, respectively. In the ERA5 reanalysis data, SAT anomalies during the NAO+ regime (Fig. 7a) are dominated by above-average temperatures over most of Eurasia as well as cold weather over the North American continent and especially over the Labrador Sea region. Anomalies of opposite sign are seen during NAO– regimes (Fig. 7d) with temperatures over 4.5 K above climatology over the Labrador Sea, Greenland, and eastern Canada. The Scandinavian Blocking regime (Fig. 7b) is characterised by warm anomalies over the northern North Atlantic between Greenland and Norway as well as over most of North America, while the northernmost regions of the American continent are slightly colder than in the climatological mean. Also most of Eurasia, except for Scandinavia, experiences below-average temperatures. During Atlantic Ridge conditions (Fig. 7c), cold weather is present over western Europe, Scandinavia, and the adjacent Atlantic Ocean towards Greenland as well as over eastern North America. Western North America and a band between the Black Sea and the Kara Sea are warmer on average. Also the North Atlantic off Newfoundland shows positive SAT anomalies.

Total precipitation anomalies during NAO+ regimes (Fig. 8a) are characterised by wet con-

ERA5

Figure 7: Composited SAT anomalies for the different WRs identified in the ERA5 reanalysis dataset using the time period 1979–2021.

ditions over the Atlantic north of 40 °N, which maximise over the British Isles and southern Scandinavia, along with dry anomalies south and west of that. Again, the NAO– regime (Fig. 8d) shows a similar but opposite picture, with dry anomalies over the northern Atlantic maximising at the east coast of Greenland and wet conditions to the south. During the Scandinavian Blocking regime (Fig. 8b), precipitation tends to be below average over western Europe, but heavy precipitation anomalies are experienced in the Denmark Strait region. The Atlantic Ridge regime (Fig. 8c) features strong dry anomalies in the area of the pronounced ridge in the geopotential height field and weaker wet anomalies around.

The correlation between Euro-Atlantic WRs and temperature and precipitation anomalies is summarised in Hertig and Jacobeit (2014) and matches the observed patterns in Figures 7 and 8 very well. For example, above-average temperatures and precipitation over northern Europe and Scandinavia were found to accompany the positive NAO phase along with dry anomalies over southern central Europe and Northwest Africa (Hurrell et al. 2003), or in the most extreme cases also heavy precipitation events over Northern Europe and drought periods in the Mediterranean region (Yiou and Nogaj 2004). During negative NAO phases, the frequency

ERA5
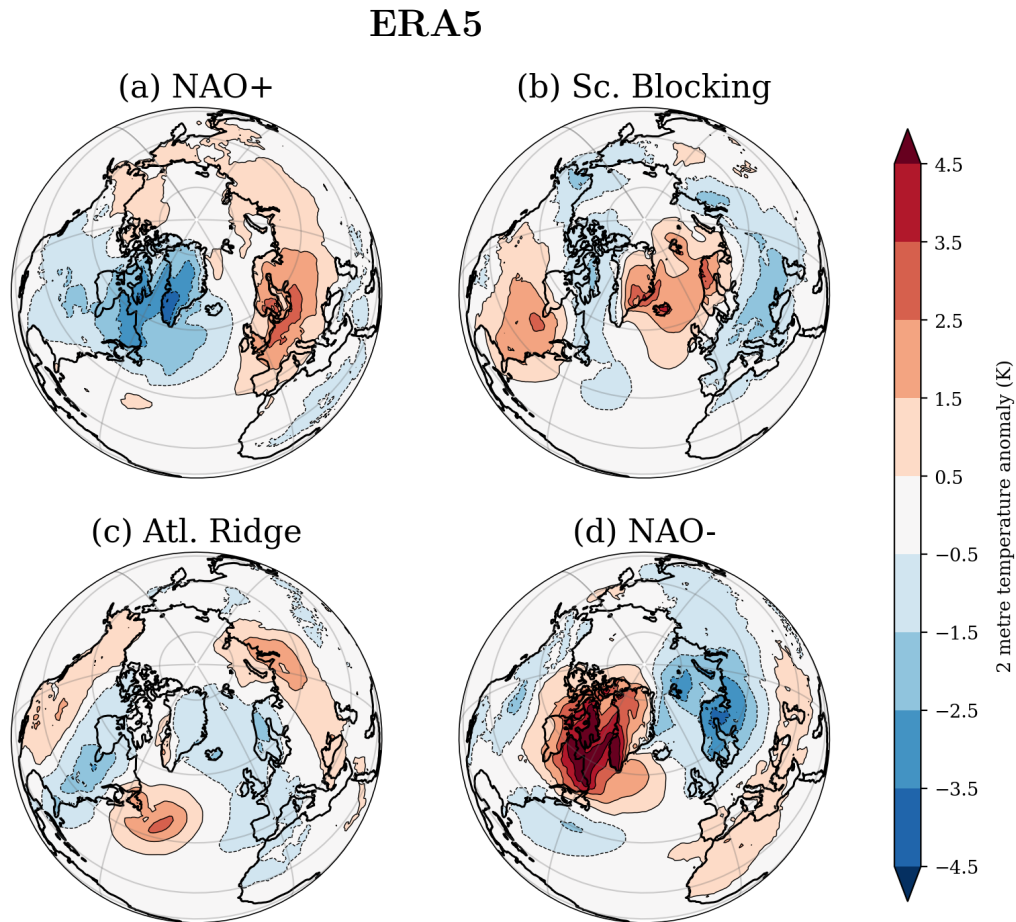
(a) NAO+

(b) Sc. Blocking

(c) Atl. Ridge

(d) NAO-
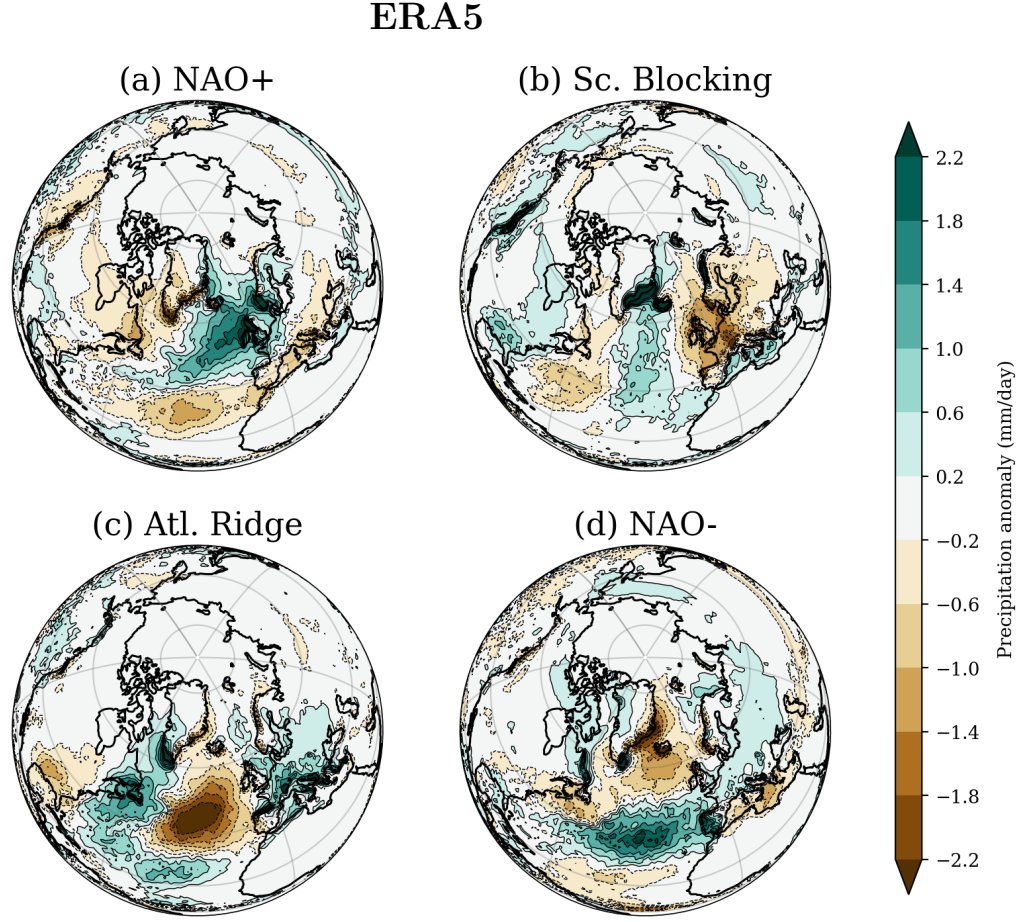
Figure 8: Composited total precipitation anomalies for the different WRs identified in the ERA5 reanalysis dataset using the time period 1979–2021.

of cold days is increased over Scandinavia and decreased over Iberia (Plaut and Simonnet 2001), and heavy precipitation events are seen over Southern Europe (Yiou and Nogaj 2004). Blocking regimes are typically associated with a warm and dry Scandinavian region and below-average temperatures over south-eastern Europe (Plaut and Simonnet 2001; Yiou and Nogaj 2004). The observed SAT anomaly patterns also agree very well with the composites of European temperature anomalies over land for the different WRs identified in the NCEP/DOE reanalysis by Cattiaux et al. (2013a), who used the observational E-OBS v3.0 dataset produced from in-situ temperature measurements.

Comparing the regime composites of SAT anomalies to the Z500 composites in Section 3 reveals that temperatures tend to be below average where we see troughs in the geopotential height field, while ridges are often accompanied by warm weather. Also for the composites of total precipitation anomalies, the regions of dry anomalies often coincide with geopotential height ridges, while heavy precipitation is often seen in regions where strong Z500 gradients meet orography (for example the strong wet anomaly at the Greenland coast during Scandinavian Blocking conditions).

Before assessing the ensemble's representation of the historical SAT and total precipitation patterns, a note on the statistical distribution of precipitation anomalies: Since precipitation does generally not follow a Gaussian normal distribution, but rather a Gamma distribution (e.g. Yiou and Nogaj 2004; Martinez-Villalobos and Neelin 2019), the majority of the daily anomalies are expected to be negative, while a few days show very heavy precipitation anomalies, which can nudge the mean towards positive values. As a logical consequence, the spatial pattern of the median of precipitation anomalies (see Figure A3 in the appendix) is heavily dominated by negative values. The only region to show a slightly positive median value is Iceland during the Scandinavian Blocking regime (Fig. A3b), which experiences strong positive precipitation anomalies in the composite mean (Fig. 8b).

4.3 Simulated historical temperature and precipitation patterns associated with different weather regimes

The same compositing procedure is applied to the SAT and total precipitation anomalies in the historical SMHI-LENS simulation to obtain Figures 9 and 11, respectively. SAT anomalies during Scandinavian Blocking regimes (Fig. 9b) are characterised by the same pattern as in the reanalysis data: warm anomalies over the northern North Atlantic surrounded by weaker cold anomalies, although both the positive and the negative anomalies show an increased magnitude compared to ERA5. Also for the Atlantic Ridge regime (Fig. 9c), the pattern resembles the one observed in ERA5 and features above-average temperatures over the Atlantic coast of Newfoundland and eastern Europe, whereas western Europe and the eastern North Atlantic as well as eastern North America experience below-average temperatures. For the NAO– regime in the SMHI-LENS (Fig. 9d), positive anomalies over eastern Canada are again present but do not reach the same magnitude as in ERA5 and are even replaced by weak cold anomalies over Greenland. During the simulated NAO+ regime (Fig. 9a), negative anomalies over the region around the Labrador Sea are weaker and much less coherent than in ERA5. Also, western Europe is not characterised by warm anomalies as in ERA5 but rather has a tendency towards below-average temperatures in northern and southern Europe.

For total precipitation anomalies, the same picture can be drawn. Again, the Scandinavian Blocking regime (Fig. 11b) with the associated wet anomaly over the Denmark Strait and dry conditions over Scandinavia, as well as the Atlantic Ridge regime (Fig. 11c), with the characteristic strong dry anomaly over the central North Atlantic and above-average precipitation in Southern Europe, are represented fairly well by the ensemble. For the Atlantic Ridge regime, anomalous heavy precipitation is considerably stronger over the Mediterranean region compared to ERA. The precipitation anomaly pattern during NAO– regimes (Fig. 11d) features dry anomalies in the northwest Atlantic and wet anomalies to the southwest that are compara-

Historical SMHI-LENS

(a) NAO+   (b) Sc. Blocking

(c) Atl. Ridge   (d) NAO-

Figure 9: Composited SAT anomalies as in Figure 7 but for the different WRs identified in the SMHI-LENS historical simulation covering the time period 1980–2010.

SSP5-8.5 SMHI-LENS

(a) NAO+   (b) Sc. Blocking

(c) Atl. Ridge   (d) NAO-

Figure 10: Composited SAT anomalies as in Figures 7 and 9 but for the different WRs identified in the SMHI-LENS future SSP5-8.5 simulation covering the time period 2070–2100.

ble in magnitude to ERA5, but shows less of the characteristic zonality as is also the case for the Z500 composites. Especially the region around the Faroe Islands is simulated to experience much wetter conditions than in ERA5. The simulated NAO+ regime (Fig. 11a) is characterised by below-average precipitation in the Bay of Biscay and weak positive precipitation anomalies over central and eastern Europe as well as over the western North Atlantic, whereas this regime is dominated by strong above-average precipitation over most of the North Atlantic in ERA5.

The observed differences in SAT and precipitation anomaly patterns between the ensemble simulations and ERA5 go along well with the differences seen in the WR patterns in Section 3. Since temperature and precipitation anomalies are correlated with the mean circulation during the different WRs, this behaviour is to be expected (Hertig and Jacobeit 2014). While Scandinavian Blocking and Atlantic Ridge are represented well, the ensemble struggles more at reproducing the NAO– and especially the NAO+ regime and the associated anomalous weather. As seen for ERA5, regions of ridges in the Z500 anomalies mostly coincide with warm and dry anomalies in the composites, while troughs are often connected to below-average temperatures and wet conditions.

4.4 Projected future temperature and precipitation patterns during different weather regimes

For the future SAT and total precipitation anomaly patterns under the high-emission SSP5-8.5 scenario, one has to keep in mind, that the anomalies are calculated with reference to the respective climatology. The anomalies shown in Figures 10 and 12 do not account for any changes in the mean climate, which was described in Section 4.1.

Under the high-emission SSP5-8.5 scenario, the SAT anomalies are generally projected to weaken (Figure 10). Compared to the simulated SAT composites in Figure 9, the patterns and the sign of the anomalies stay the same but are weakened in amplitude for all four WRs. This is particularly the case for the previously pronounced warm anomalies during the Scandinavian Blocking regime (Fig. 10b) over the northern North Atlantic of over 4.5 K in some places, that mostly stay below 2.5 K in the future climate.

The decrease in the magnitude of SAT anomalies compared to the historical simulation is in line with the decrease seen in the Z500 anomaly patterns. A change in the Z500 gradient affects the intensity of the large-scale flow and the advection of warm and cold air masses by the mean circulation (Hurrell et al. 2003).

The total precipitation anomalies, however, are rather seen to increase in magnitude for most of the regimes under the strong warming scenario. The NAO+ regime's dry anomalies over the Bay of Biscay (Fig. 12a) increase slightly and are opposed by stronger wet anomalies to

Historical SMHI-LENS

Figure 11: Composited total precipitation anomalies as in Figure 8 but for the different WRs identified in the SMHI-LENS historical simulation covering the time period 1980–2010.

SSP5-8.5 SMHI-LENS

Figure 12: Composited total precipitation anomalies as in Figures 8 and 11 but for the different WRs identified in the SMHI-LENS future SSP5-8.5 simulation covering the time period 2070–2100.
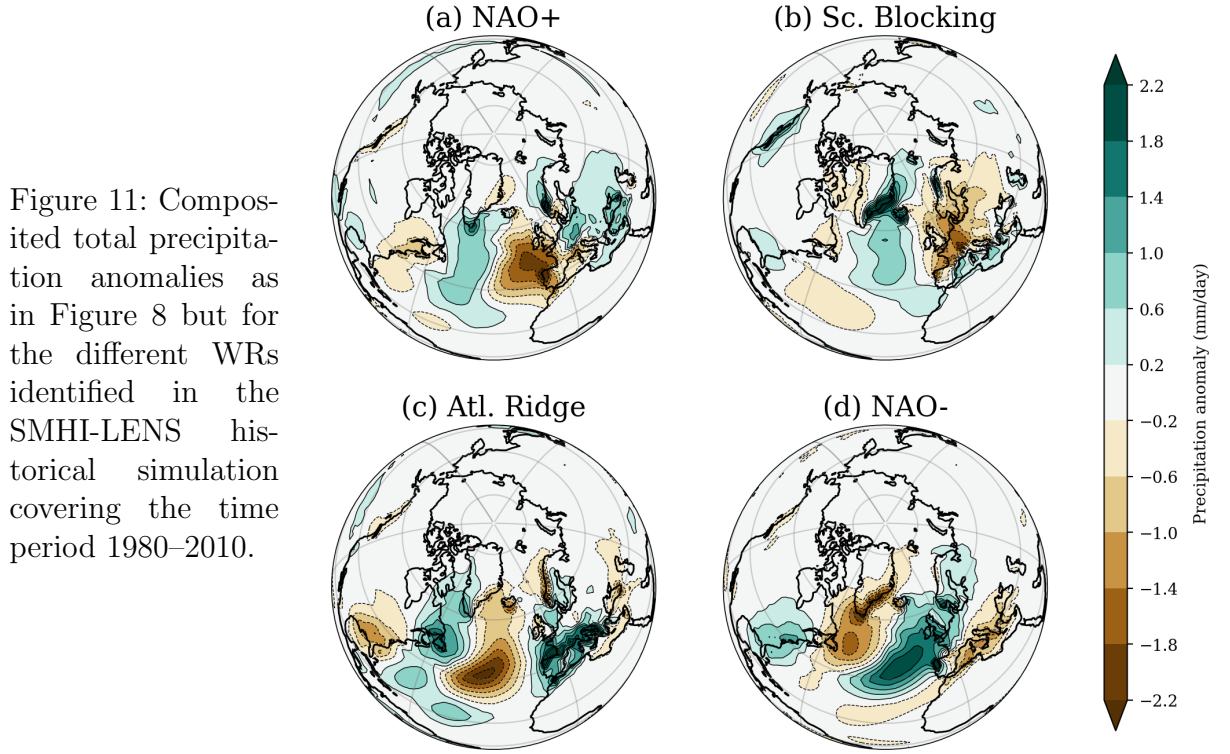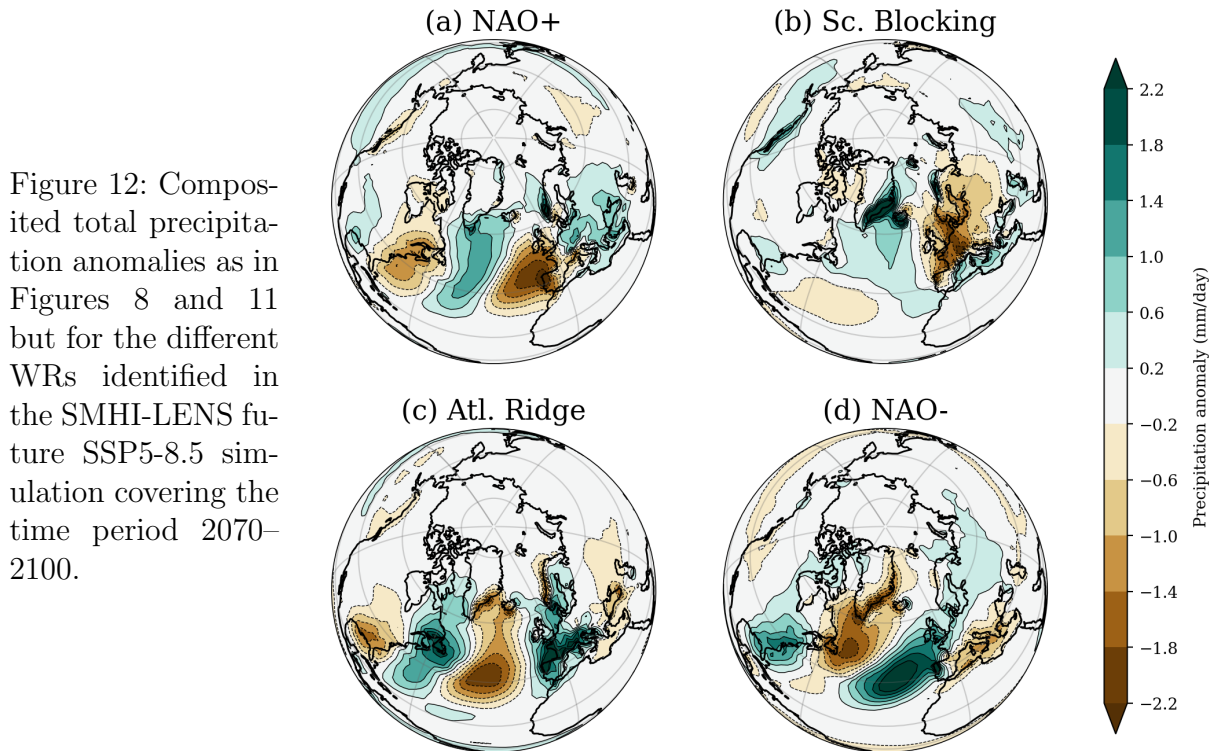
the west. During the Scandinavian Blocking regime (Fig. 12b), the dry anomalies over central and northern Europe increase in the future simulation, while the strong wet anomalies over the Denmark Strait region persist. The dry Atlantic Ridge (Fig. 12c) is projected to have slightly less strong dry anomalies, but the wet anomalies to the east and the west intensify. The NAO– regime (Fig. 12d) experiences a strong increase in heavy precipitation over the eastern North Atlantic along with a strengthening of the dry anomalies in the western North Atlantic.

This increase in the magnitude of precipitation anomalies agrees well with the generally enhanced atmospheric water vapor content under global warming expected from the Clausius-Clapeyron relationship and the enhanced precipitation variability on daily to decadal timescales identified in CMIP5 models and two climate model large ensembles under RCP8.5 forcing (Pendergrass et al. 2017). Also, it aligns well with the observation of wet-gets-wetter and dry-gets-drier as described for the mean climate in Section 4.1 (compare Held and Soden 2006).

The close connection between the WRs identified in the previous section and SAT and precipitation anomaly patterns described in this section confirms the relevance of the WR framework for describing the Euro-Atlantic weather and circulation.

5 Projected changes in extreme weather during weather regimes

After looking at the changes in mean temperature and precipitation that are associated with the different weather regimes, this section presents the simulated changes in hot and cold, as well as wet and dry extremes related to the WR framework.
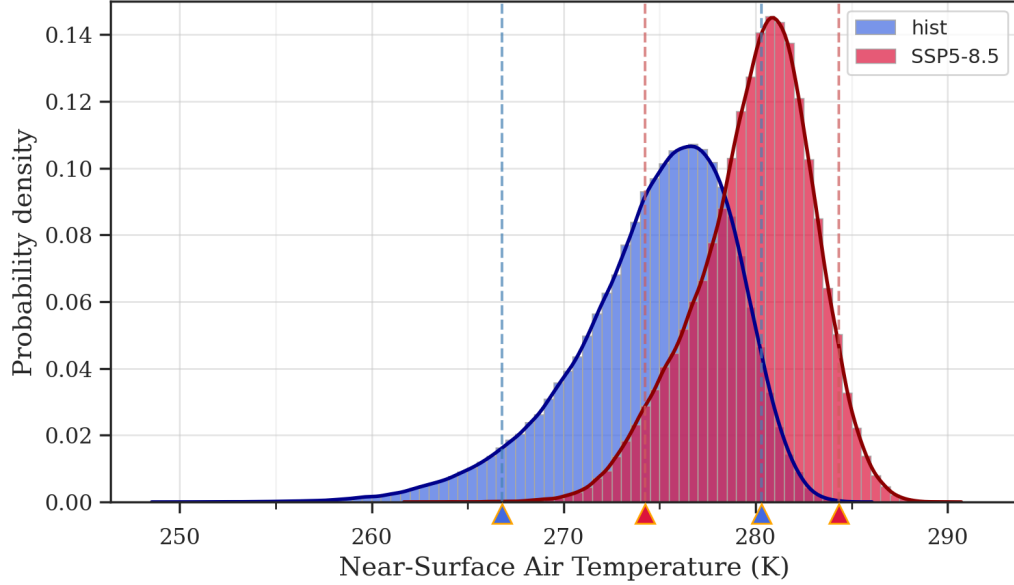
Figure 13: Histogram of wintertime (DJF) SAT at 54 °N, 10 °E for the historical and future simulation of the SMHI-LENS. The smoothed curves are kernel density estimates of the distribution. The triangles below the x-axis indicate the temperatures corresponding to the 5th and 95th percentiles.

Figure 13 shows the probability distribution of SAT in the SMHI-LENS historical and future scenario simulations at 54 °N, 10 °E, which corresponds to a location close to the city of Neumünster in Northern Germany. This serves as an example of how the statistical distribution is connected to the definition of extreme events and how they are projected to change under climate warming. The 5th percentile serves as the threshold to cold extremes, while SAT values above the 95th percentile are counted as warm extremes. This means that 90% of the simulated SAT values are within the range between the lower and the upper threshold.

As can be seen in the example of the SAT distribution at the chosen location, both the mean and the width of the distribution change under the future SSP5-8.5 scenario. The mean increases notably, whereas the distribution width gets narrower. While the difference between the thresholds for cold and hot extremes is around 14 K for the historical simulation, it decreases to around 10 K under the SSP5-8.5 by the end of the century.

In the following, the focus will be on comparing the extremes relative to the respective clima-

tological mean of the historical and the future simulation of the SMHI-LENS. So, rather than looking at shifts in the distribution mean, changes in the extreme percentiles of the anomaly distributions are assessed. This is achieved by using the historical 5th and 95th percentiles as thresholds for the future SSP5-8.5 scenario simulation as described in the Methods (Section 2.2.2).

5.1 Changes in extreme near-surface temperature

The probability of exceeding the historical SAT threshold value in the future ensemble simulation is shown for cold extremes in Figure 14 and for warm extremes in Figure 15. Since the thresholds are given by the 5th and 95th percentiles, values below 5% indicate that reaching extremes of the same magnitude is less likely, or in other words, extremes get less extreme. For values above 5% probability, the occurrence of extremes of historical magnitude is more probable, thereby implying that more extreme values get more likely.

Over most of the northerly latitudes (north of 40 °N), the same trend for all WRs and both warm and cold extremes is seen: a decrease in probability indicating that extremes of the same magnitude as during the historical simulation get less extreme or less likely. This general trend indicates that, for most regions, the distribution gets narrower under the SSP5-8.5 scenario simulation.

Cold extremes (Fig. 14) experience the strongest decrease in magnitude or probability in the region of the historical winter sea ice edge (as seen e.g. in the median March sea ice extent for the period 1981–2010 in Meier et al. (2021)), namely in the Bering, Chukchi and Okhotsk Sea, the Laptev, Kara and Barents Sea and the Greenland and Labrador Sea. In these regions, the probability mostly drops to 0%, indicating that extreme cold events of historical magnitude relative to future climate are not to be expected from the ensemble simulations. The location of this strong decrease gives rise to the assumption that these changes in cold extremes are related to changes in Arctic sea ice. The winter sea ice extent is seen to vary between years, leading to a fluctuating sea ice edge (Meier et al. 2021). Since the surface temperatures are very different for open ocean or sea ice and snow, these changes in sea ice will be heavily reflected in SAT anomalies along the sea ice edge. Under the high-emission SSP5-8.5 simulation, Arctic sea ice is projected to decrease drastically (Wyser et al. 2021). This makes the assumption plausible, that the region of the mean historical sea ice edge will be constantly characterised by open ocean, thereby decreasing the variability in surface temperatures and decreasing the magnitude and likelihood of cold extremes.

The probability of surpassing the historical threshold for warm extremes (Fig. 15) decreases for nearly the entire region encircled by the winter sea ice edge to values close to or at 0%. Likewise, Scandinavia and the Ural region experience less warm extremes in the future simulation. As

Cold extremes

(a) NAO+   (b) Sc. Blocking

(c) Atl. Ridge   (d) NAO-

Figure 14: Probability of reaching cold extremes corresponding to the historical 5th percentile of SAT anomalies in the SMHI-LENS SSP5-8.5 simulation for the four weather regimes identified for the period 2070–2100.

Probability TAS$_{SSP5}$ < TAS$_{hist}^{5^{th}}$ (%)

Warm extremes

(a) NAO+   (b) Sc. Blocking
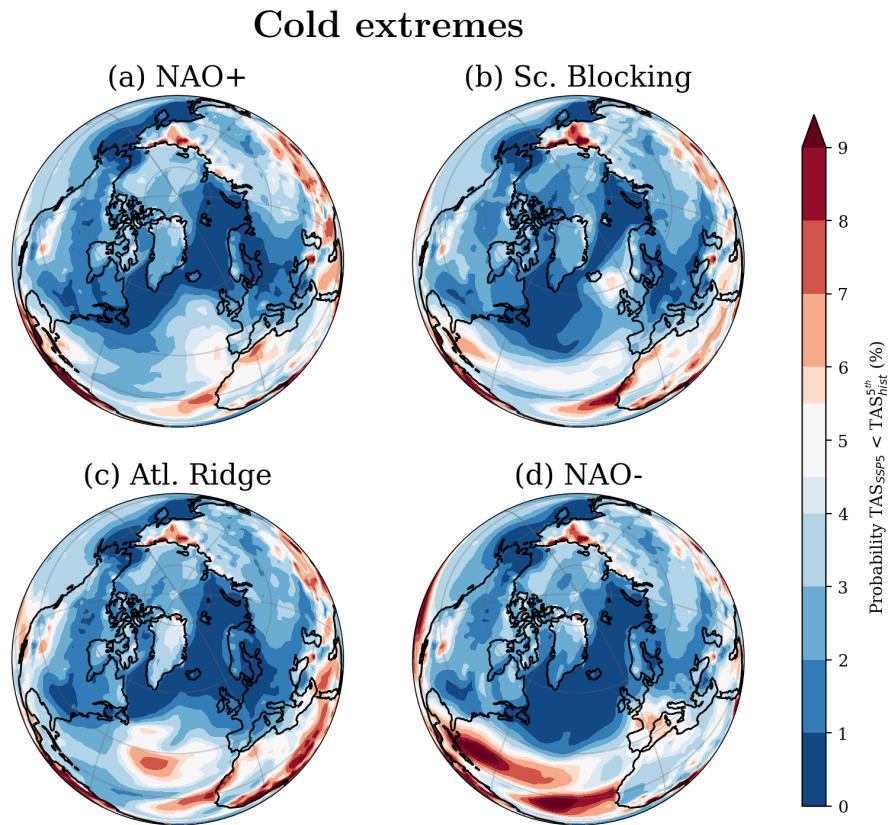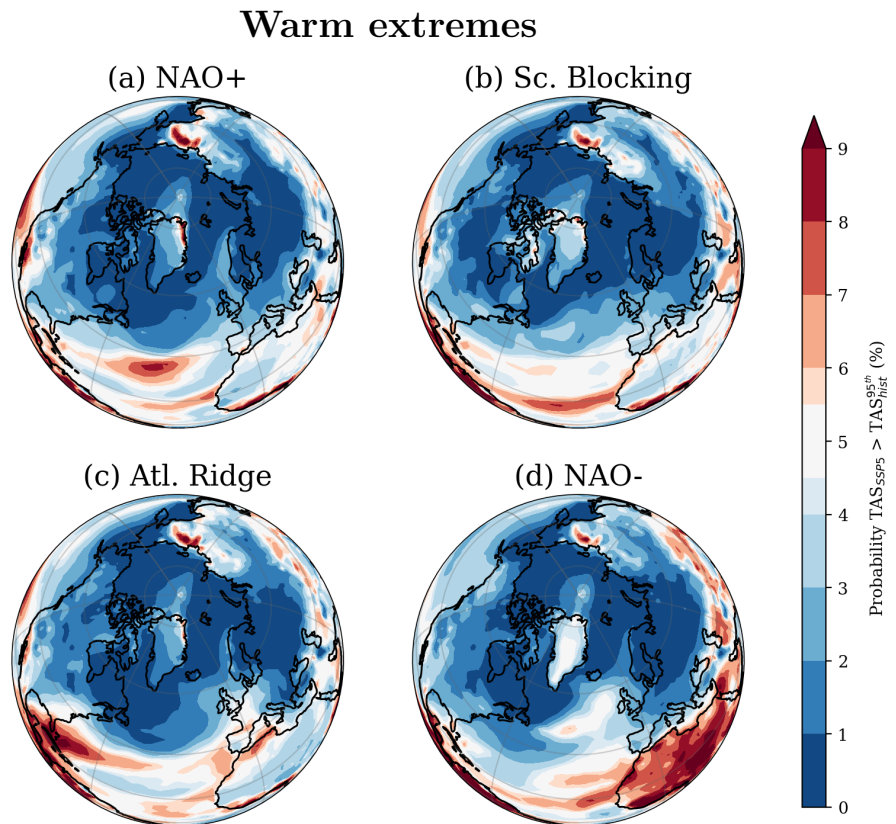
(c) Atl. Ridge   (d) NAO-

Figure 15: As in Figure 14, but for the probability of reaching historical warm extreme values corresponding to the 95th percentile of SAT anomalies.

Probability TAS$_{SSP5}$ > TAS$_{hist}^{95^{th}}$ (%)

for cold extremes, a connection between this decrease in the probability of warm extremes and the melting of Arctic sea ice seems likely. Following the same reasoning as above, the projected decrease in sea ice reduces the SAT variability over most of the Arctic and thereby the probability of extreme warm events. Only the region between Ellesmere Island, Lincoln Sea, and the North Pole shows a weaker decrease in probability. In the current climate, this region is still characterised by relatively thick multiyear sea ice (Meier et al. 2021), and climate simulations with strong forcing scenarios show that the sea ice in this region is often projected to be last to melt completely (Koenigk et al. 2013; Wei et al. 2020). If this is also the case for (some of) the SMHI-LENS simulations, this could explain a weaker decrease in SAT variability and hence warm extremes as seen in Figure 15 for all WRs.

Regional differences between the WRs are present, especially over the Atlantic Ocean and over Europe and North Africa. The most pronounced differences away from the Arctic region are seen for the NAO– regime (Figs. 14d and 15d). While the probability of cold extremes decreases slightly over North Africa, the probability of warm extremes increases to over 9% in some places for the same region, indicating a distortion of the SAT distribution towards a distribution with a more positive skewness (i.e. the right tail gets longer). The composited mean SAT anomalies in Figures 9d and 10d did not show any remarkable changes for this region. Intriguingly, warm extremes during NAO– phases (Fig. 15d) over Greenland are almost unchanged, whereas extremes of historical magnitude are getting less likely over Greenland for the other regimes. Over the Atlantic Ocean south of 40 °N, cold extremes during negative NAO experience a strong increase in two bands: east of the Caribbean and west of Cape Verde. Also the Mediterranean region sees a weak increase. North of these bands of increased probability, the North Atlantic shows a probability of 0% for cold extremes of historical magnitude.

The NAO+ regime's warm extremes (Fig. 15a) experience an increase in probability over the middle of the North Atlantic just south of 40 °N, whereas the strong decrease over the Ural region is seen to spread further east over Asia than during the other WRs. Cold extremes during positive NAO phases (Fig. 14a) are characterised by a reduction in probability along the historical sea ice edge that is mostly in line with the general changes described before.

The Scandinavian Blocking regime shows a slight increase in cold extremes (Fig. 14b) between Iceland and the British Isles, which corresponds to the region that is characterised by a decrease in the magnitude of positive SAT anomalies in the composite mean (Figs. 9b and 10b). This regime's changes in the probability of warm extremes (Fig. 15b) agree well with the general decrease seen for all regimes with a weaker reduction over Greenland compared to the positive NAO and the Atlantic Ridge regime.

During Atlantic Ridge regimes, cold extremes (Fig. 14c) get slightly more extreme or likely in the middle of the Atlantic just south of the location of the ridge in the Z500 anomaly field.

Also tropical Africa experiences an increase in the probability of cold extremes of historical magnitude that is not seen during the other regimes, while cold extremes over Greenland decrease less compared to the other WRs. Warm extremes during Atlantic Ridge regimes (Fig. 15c) are considerably more probable over the Caribbean region and the adjacent western North Atlantic. In contrast to the other regimes, the Iberian peninsula and France during Atlantic Ridge conditions experience weak changes and even an increase in warm extremes over northern Morocco and Algeria.

Some of the regional WR differences can be related to the changes seen in the composite mean (Figs. 9 and 10). Regions that are characterised by a decrease in positive SAT anomalies under SSP5-8.5 forcing tend to show a (weak) increase in the probability of cold extremes (as e.g. in the Mediterranean region during NAO– phases), while some of the regions characterised by cold SAT anomalies in the composite mean show an increased probability for warm extremes compared to the other regimes (as is the case for the Labrador Sea region during Scandinavian Blocking regimes).

5.2 Changes in extreme precipitation

Repeating the same analysis for precipitation anomalies yields the changes in the probability of dry extremes in Figure 16 and of wet extremes in Figure 17. Again, extremes are defined by the simulated historical 5th and 95th percentiles.

Generally, dry extremes are projected to become more likely for most of the Northern Hemisphere during all WR conditions with probabilities increasing to over 16% for some regions. Also wet extremes are seen to increase in probability over the Arctic Ocean, Siberia, and Asia during all WRs. The subtropical Atlantic, on the contrary, experiences a decrease in the probability of both dry and wet extreme events of historical magnitude. Moreover, the region just south of Iceland shows a lower probability of dry extremes for all regimes, which is in strong contrast to the surrounding pronounced increase.

These general changes in the probability of extreme events align with the simulated changes in mean climate: especially the occurrence of wet extremes agrees well with the mean SAT changes (Fig. 5). This could be understood in the context of an increasing hydrological cycle in response to enhanced atmospheric water vapour content in a warmer climate (Held and Soden 2006), especially in the Arctic region, which in addition is influenced by AA and sea-ice loss (McCrystall et al. 2021).

The changes in dry extremes, on the other hand, appear to also be connected to the mean precipitation changes. As described in Section 4.1, Arctic precipitation is enhanced in the warmer future climate and this elevated mean in total precipitation also makes more extreme

dry events possible (since negative precipitation values are nonexistent, the mean precipitation value sets the upper bound for the magnitude of dry extremes). The subtropical North Atlantic and the region just south of Iceland, on the other hand, are characterised by less precipitation in the future climate as well as less intense dry extremes (Fig. 16).

As for the SAT extremes described in the previous section, regional differences between the WRs are also present for both wet and dry extremes. During the Scandinavian Blocking regime, the probability of wet extremes (Fig. 17b) only increases slightly over Scandinavia and western Europe, while the probability of dry extremes (Fig. 16b) experiences a strong increase of over 10 percentage points. The Atlantic Ridge regime is characterised by an increase in the probability of dry extremes over Southeastern Europe (Fig. 16c), while, at the same time, wet extremes over Scandinavia and the British Isles are becoming more likely (Fig. 17c). During NAO− phases, dry extremes (Fig. 16d) experience the same general increase in probability at northern latitudes as during the other regimes although the changes over land are comparably weak over Canada, Alaska, and Eurasia. Changes in the probability of wet extremes during NAO− conditions (Fig. 17d) show at the most only a weak increase or no change for the North Atlantic region around and south of Iceland, whereas the NAO+ regime's probability of wet extremes (Fig. 17a) increases consistently in this area. The enhanced probability of dry extremes over the Arctic Ocean is even more consistently exceeding 16% during positive NAO conditions (Fig. 16a) compared to the other regimes.

The regional differences in the probability changes are in line with the changes in the mean total precipitation composites in Figures 11 and 12. Stronger dry anomalies in the precipitation composites under the SSP5-8.5 scenario tend to align with strong increases in the probability of dry extremes and comparably weak or no increases for wet extremes, for example for the Scandinavian region during Scandinavian Blocking regimes. The regions that are more likely to experience wet extremes, however, are more often characterised by (intensifying) positive precipitation anomalies in the composites, as seen for southwestern Europe during the Atlantic Ridge regime.

All in all, the general direction of the projected changes in extreme surface weather is opposite for temperature and precipitation. This is most pronounced over the Arctic region. While SAT extremes over most of the northerly latitudes are projected to get less extreme relative to the simulated future climate, the precipitation extremes experience an intensification over the same region. These changes are indicative of modifications of the probability distributions in the form of a more narrow SAT distribution and a wider precipitation distribution (although one has to keep in mind its non-Gaussian shape). At more southerly latitudes, these changes are mostly more moderate or even of opposite sign. Regionally, differences from these general changes are seen when looking at individual WRs and are often in accordance with the changes in the SAT and precipitation composite means.

Dry extremes

(a) NAO+ | (b) Sc. Blocking

(c) Atl. Ridge | (d) NAO-

Figure 16: Probability of reaching dry extremes corresponding to the historical 5th percentile of total precipitation anomalies in the SMHI-LENS SSP5-8.5 simulation for the four weather regimes identified for the period 2070–2100. Note the unevenly spaced colormap that is different from Figures 14, 15 and 17.
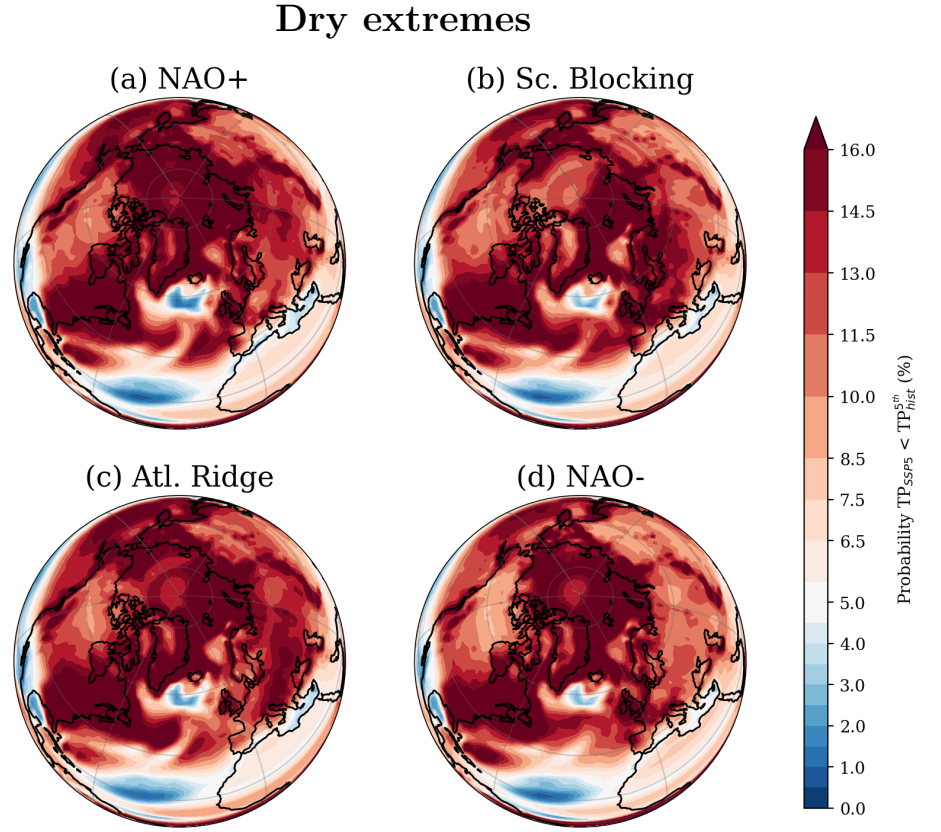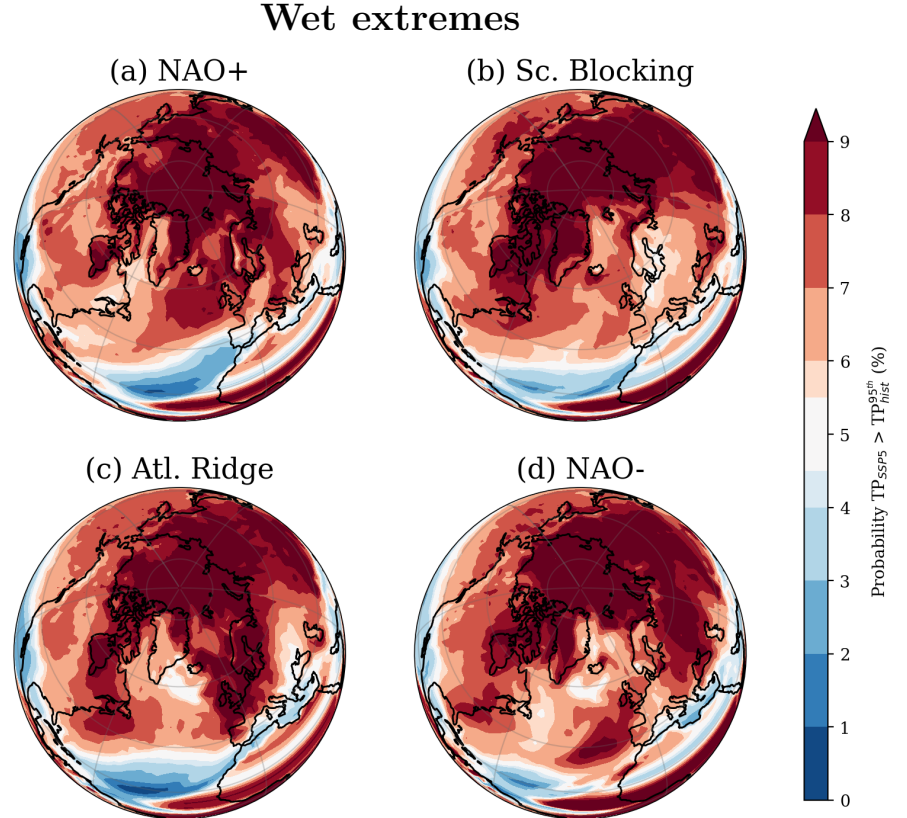
Wet extremes

(a) NAO+ | (b) Sc. Blocking

(c) Atl. Ridge | (d) NAO-

Figure 17: As in Figure 16, but for the probability of reaching historical wet extreme values corresponding to the 95th percentile of total precipitation anomalies.

6 Discussion

In the following, the results described in Sections 3, 4, and 5 are discussed in a more general context. The first discussion question is about the representation of WRs in current state climate models along with possible biases. This is followed by an assessment of the simulated future changes, before putting the connection to surface weather and extreme events into context.

6.1 How well do climate models represent weather regimes?

Overall, the EC-Earth3 model used for the SMHI-LENS was found to have reduced biases in DJF compared to the previous version (EC-Earth2) used in the CMIP5 effort (Döscher et al. 2021). Nonetheless, significant biases in climatological mean SAT and precipitation are still present, especially over the North Atlantic region (see Section 4.1). The North Atlantic jet is still displaced poleward and shows a too-penetrative pattern over Europe compared to observations. Moreover, winter European blocking frequency is underestimated in comparison to observational data. Also the March sea ice concentration is generally too high in EC-Earth3 compared to satellite observations in the Greenland Sea, the Labrador Sea, and the Eastern Barents Sea (Döscher et al. 2021).

A recent study by Delgado-Torres et al. (2022) specifically investigated the representation of Euro-Atlantic WRs in a ten-member ensemble performed with EC-Earth3.3. Using non-initialised historical simulations, they compared the simulated regime patterns to two different reanalysis products, the Japanese 55-year Reanalysis JRA-55 and the NCEP/NCAR Reanalysis. Independently calculating the WRs for each dataset, they found high correlations between EC-Earth3 and the reanalysis data for all winter regime patterns - higher and more consistent than the correlations in this thesis. However, their algorithm differs from the methodology used here: Days that do not distinctly belong to any of the clusters were filtered out by applying minimal-correlation and minimal-persistence filters to their projected daily maps. This additional step and the application of the clustering algorithm to sea level pressure instead of Z500 anomalies are possible explanations for more observation-consistent results in their study compared to this thesis. Delgado-Torres et al. (2022) chose specifically sea level pressure because it is less affected by global warming compared to geopotential height.

Also by using the approach of pseudo Principal Components (pseudo-PCs) (i.e. projecting the simulated geopotential height fields onto the regime patterns identified in a reference dataset, often reanalysis data), more consistent results between reanalysis and model data can be found in the literature (e.g. Ullmann et al. 2014; Wiel et al. 2019; Fabiano et al. 2020). This is expected from this methodology, which is employed to ensure high levels of spatial similarity between the different datasets (see the explanation in Wiel et al. 2019). With this approach,

one can investigate the model's ability to reproduce the known WRs and conveniently analyse changes in regime statistics. Since the focus of this thesis is on identifying the regimes and their potential changes in a future climate, the use of pseudo-PCs was omitted on purpose not to take present-day data as a reference.

In contrast to using pseudo-PCs, this thesis has focused on the spatial patterns that are inherent to the different datasets. This technique must be understood, however, taking into account that horizontal resolution has been identified as an important factor in allowing climate models to capture the Euro-Atlantic regimes in previous systematic assessments of the representation of regime patterns. Dawson et al. (2012) evaluated the regime patterns in the ECMWF IFS model Cy36r1 in a high-resolution configuration integrated at T1279 resolution (corresponding to ca. 16 km grid spacing) and a low-resolution configuration (T159, corresponding to ca. 125 km). They found that the low-resolution version of the same global atmospheric model performs much worse at representing the regime patterns compared to the high-resolution counterpart: in the T159 configuration only the positive and negative NAO phases were identified, whereas the T1279 configuration features all four regimes and reproduces the spatial patterns accurately. Dawson and Palmer (2015) suggested that some improvements can already be achieved with an intermediate resolution configuration of the same model (T511, corresponding to ca. 40 km) in comparison with the low-resolution setup, especially in the temporal characteristics such as regime persistence and frequency.

Both studies used one model with a single member at each resolution and all model runs were performed with IFS Cy36r1 (a different version of the atmospheric model used in ERA5 and EC-Earth3), leaving open the possibility still that their findings were model-dependent. This question was addressed by Strommen et al. (2019) in their study of the impact of resolution on three different models with three members each, with one of these models being EC-Earth3.1. In addition, they investigated the impact of using an ensemble by concatenating the individual ensemble members, which agrees with the way the SMHI-LENS is used in this thesis. They found that models with weaker regime structures require a larger sample size to diagnose regimes robustly and that no systematic improvement in the spatial patterns could be observed with increasing resolution, although some regime characteristics like sharpness and persistence (of the Scandinavian Blocking regime) were represented more accurately.

Additionally, quite some work has been devoted to studying the representation of blocking events in climate models, also in the Euro-Atlantic region (e.g. Schiemann et al. 2017; Davini and D'Andrea 2020). Although improvements with increasing resolution were observed in different atmospheric GCMs and CMIP model generations, even the latest CMIP generation (CMIP6) still underestimates winter European blocking frequencies. To be precise, no model that was evaluated by Davini and D'Andrea (2020) managed to attain the observed blocking frequency.

Altogether, there seems to be potential for an improved representation of WRs with increased resolution, at least to some extent. This could be due to the better representation of orography and Rossby wave-breaking processes, which help to maintain persistent anomalies, at higher spatial resolutions (compare conclusions in Dawson and Palmer (2015)). However, considering the variety of outcomes in the studies named before, the impact of a higher resolution could be model-dependent and different for the individual regime statistics. The horizontal resolution of the SMHI-LENS with EC-Earth3, which is ca. 80 km for the atmospheric component, corresponds to double the intermediate-resolution grid spacing in Dawson and Palmer (2015). Hence, following their arguments, it could potentially perform worse than higher-resolution configurations. However, this thesis made use of a large ensemble of model runs, which could help to identify the regimes more robustly (Strommen et al. 2019). So, albeit possibly representing the regimes better than a low-resolution model with only one member, there might still be a lot of room for improvement considering the spatial resolution of the SMHI-LENS.

Nevertheless, it is also likely that increasing the horizontal resolution alone would not solve all current errors. More and more studies also point to the role of biases in the mean fields as a source of uncertainty in the representation of WRs. Especially reducing biases in sea surface temperature (SST) has been identified as a possible step to further decreasing the negative blocking frequency bias (Scaife et al. 2011; Davini and D'Andrea 2020; Fabiano et al. 2020). As described in Section 4.1, climatological mean SAT biases in the SMHI-LENS are quite pronounced over the North Atlantic region and possibly a result of the overestimation of winter sea ice concentration and thickness (Döscher et al. 2021). This also suggests considerable SST biases in this region and it appears conceivable that these biases contribute to the misrepresentation of the regime patterns by substantially impacting the synoptic-scale circulation and thereby all WRs in this region (Scaife et al. 2011; Strommen et al. 2019).

Furthermore, WRs, and also blocking in particular, are linked to the position of the jet stream (Woollings et al. 2010; de Vries et al. 2013; Madonna et al. 2017; Pasquier et al. 2019). Analysing the wintertime North Atlantic eddy-driven jet stream typically yields three preferred latitudinal positions that agree well with three Euro-Atlantic WRs (Woollings et al. 2010). Extending these findings, Madonna et al. (2017) seamlessly connected the eddy-driven jet perspective with the WR framework for the Euro-Atlantic region. They identified four clusters in both approaches and found that the Atlantic Ridge regime features a preferred northern jet location, the zonal regime (corresponding to the NAO+ phase) is connected to a central jet state, the Greenland Anticyclone (matching the NAO– regime) coincides with a southern jet location, and the European/Scandinavian Blocking pattern corresponds to a mixed jet cluster. This mixed cluster is characterised by a split or strongly tilted North Atlantic jet (Madonna et al. 2017).

Interestingly, a recent study by Dorrington and Strommen (2020) has stressed the role of jet speed variability in determining stable regimes. By filtering out the linear variability of the

eddy-driven jet, Dorrington et al. (2022) identified regimes in the Z500 field linked to the spatial features of the jet stream and its latitudinal position instead of variations in the jet speed. This means that there are very different roles for the latitudinal and longitudinal jet variability in determining WR patterns: the latitudinal position is closely linked to the individual regime patterns thereby supporting the regime classification (Woollings et al. 2010; Madonna et al. 2017). By contrast, the longitudinal variability (characterised by the jet speed) generally rather obscures the clustering results due to its strong projection on the Z500 field, which conversely offers the possibility to identify more stable regimes by filtering out jet speed variations (Dorrington and Strommen 2020; Dorrington et al. 2022). Dorrington and Strommen (2020) even suggest decomposing the Euro-Atlantic circulation into one linear mode corresponding to a zonal flow as described by the NAO+ phase and three regimes, which describe nonlinear and persistent deviations from the linear mode. Intriguingly these three stable regimes correspond to the regimes in the historical SMHI-LENS simulation that resemble the observed patterns in the ERA5 reanalysis. Taking these findings into account, one may speculate that the deviation of the simulated from the observed NAO+ pattern could be a result of a misrepresentation of the strength of the North Atlantic jet stream and its variability in the SMHI-LENS with EC-Earth3, but this would require further investigation to confirm.

All in all, previous studies along with the results in this thesis suggest that the differences between model and reanalysis could be a result of the North Atlantic biases in SAT and SST, as well as a bias in the North Atlantic eddy-driven jet stream. Considering that the atmospheric spatial resolution in the SMHI-LENS is close to the lower range of resolutions evaluated in Dawson et al. (2012) and Dawson and Palmer (2015), and taking into account the considerable biases in the Euro-Atlantic sector and especially in the North Atlantic storm track region, the representation of the WR patterns in the SMHI-LENS with EC-Earth is surprisingly good. The ensemble simulates four regime structures and three out of the four regimes resemble the observed patterns reasonably well. Only the observed NAO+ regime could not be reproduced by the model.

6.2 How do future changes in weather regimes relate to changes in tropospheric weather?

The response of the Euro-Atlantic WRs to climate change has been rather conflicting in earlier studies, as outlined in the Introduction, and most of these results are not consistent with the changes seen in this thesis either. Studies have largely been devoted to investigating changes in regime statistics by using the approach of pseudo-PCs. Cattiaux et al. (2013a) found an increase in NAO– frequency in CMIP5 models, which is in contrast to a decrease seen in the SMHI-LENS. At first glance, the results by Hertig and Jacobeit (2014) appear to agree with

the findings in this thesis for the regime responses to climate change: both the NAO+ and the Atlantic Ridge regime are projected to occur more frequently in the former, which is in line with slightly higher frequencies of occurrence in Section 3. Considering that the NAO+ regime identified in the SMHI-LENS does not resemble the observed pattern and that Hertig and Jacobeit (2014) used the pseudo-PCs approach, this agreement appears to be rather by chance however. The same applies to the increase in NAO+ frequency identified by Fabiano et al. (2021). No significant long-term trend in regime frequencies was found in Ullmann et al. (2014), but the high-pressure anomaly over the Azores during Atlantic Ridge regimes was seen to strengthen. This is in contrast to a weakening of the ridge in the geopotential height field seen during this regime under the SSP5-8.5 scenario as simulated by the SMHI-LENS.

Even more literature exists on the effect of climate change on blocking activity and there seems to be general agreement on a reduction in winter blocking frequency in strong warming scenarios (de Vries et al. 2013; Davini and D'Andrea 2020; Bacer et al. 2022). However, Masato et al. (2014) found a slight increase in Atlantic blocking frequency, which agrees with the more frequently occurring Atlantic Ridge regimes in the SSP5-8.5 SMHI-LENS simulation (Fig. 4), and no changes for European blocking in four CMIP5 models under RCP8.5 forcing. In line with the former studies, the SMHI-LENS under the SSP5-8.5 scenario simulates a reduction in Scandinavian Blocking frequency of roughly 1% (compare Figures 3 and 4). Davini and D'Andrea (2020) even suggested that the actual response in blocking frequency reduction might be stronger than projected by current CMIP models considering the under-representation of simulated blocking frequency for historical periods and that models with higher frequencies of occurrence project larger reductions (Davini and D'Andrea 2020). In the spatial patterns of winter European blocking events, Kennedy et al. (2016) and Nabizadeh et al. (2021) identified a general, yet spatially nonuniform, strengthening of the Z500 anomalies under future warming scenarios. This strengthening is not confirmed by the future simulation with the SMHI-LENS seen in Figure 4. Additionally, disagreement exists on a possible spatial translation of the blocking centres, also in the literature: While the Z500 response was noticeably shifted westward in Nabizadeh et al. (2021), an eastward shift was reported by Masato et al. (2014). Neither the Atlantic Ridge nor the Scandinavian Blocking is seen to move under the SSP5-8.5 scenario in this thesis.

Generally, as mentioned in the introduction, the common methodology in previous studies of responses of WR patterns to climate change was based on projecting the future fields on the reduced phase space obtained from present-day reference data (i.e. the pseudo-PCs approach). These studies thereby ignore variability in the spatial patterns, since particular regime patterns from the reference dataset are prescribed. This approach is often motivated by an early study by Palmer (1999), who found geographical regime structures to be unaffected by the external forcing both in theoretical considerations and GCM integrations. There, the system responded

primarily through changes in regime statistics (Palmer 1999). This prompted following studies to characterise the WR response to climate change in terms of changes in regime occurrence and persistence (Cattiaux et al. 2013a; Ullmann et al. 2014; Fabiano et al. 2021). However, this approach breaks down if the regimes experience spatial changes or if the regime patterns are not represented correctly in climate models, thereby likely introducing additional uncertainties, as elucidated in detail in Dorrington et al. (2022). These considerations served as one major motivation for the methodology applied in this thesis: By not prescribing regime structures for the SMHI-LENS simulations, new WR patterns can evolve. However, as seen in the misrepresentation of the NAO+ regime in the historical simulation, this again introduces new challenges in the interpretation of the results for the future scenario. Nevertheless, since the general weakening of anomalies in the Z500 composites in the future simulation is quite consistent for all regimes, this allows for confidence that similar changes can be expected for the observed NAO+ pattern.

As described before, there is a close connection between the position of the North Atlantic eddy-driven jet stream and Euro-Atlantic WRs. Hence it appears logical that jet changes might lead to changes in these WRs (Dorrington et al. 2022). Furthermore, the position of the North Atlantic jet stream is directly associated with the North Atlantic storm track: the jet streams are just to the south of the storm tracks (Madonna et al. 2017) and, in the time mean, storm tracks and jet stream closely follow one another (Löfverström 2020). Changes in the position and the intensity of storm tracks, on the other hand, are related to the response of the mid-latitude temperature gradient to climate change (Shaw et al. 2016). Moreover, spatial changes in WR patterns have been seen to be associated with jet and storm track changes in model simulations (Piazza et al. 2016). Here a lot of uncertainty in future projections comes into play: The mid-latitude temperature gradient is subject to competing processes, leading to a tug-of-war on the response of the storm tracks (Shaw et al. 2016; Catto et al. 2019; Yu et al. 2023). While the warming of the tropical upper-troposphere due to enhanced latent heat release in tropical convection as well as ocean warming at lower latitudes acts to increase the meridional temperature gradient, intensify and push the mid-latitude jet poleward, Arctic surface warming that is enhanced by AA can be seen to have the opposite effect on the jet stream and storm tracks (i.e. a weakening and equatorward shift) (Shaw et al. 2016; Peings et al. 2017). The actual response to climate change will depend on the relative influence of these competing processes. However, there is emerging evidence for a more zonal mid-latitude circulation along with a squeezing of the North Atlantic jet under a changing climate, which could reconcile the tug-of-war between the opposing effects of upper-tropospheric warming and AA (Barnes and Polvani 2013; Peings et al. 2017; Peings et al. 2018).

A zonalisation of the mid-latitude circulation and the storm tracks was also seen in the SSP5-8.5 simulation with the SMHI-LENS in this thesis (Fig. 6) along with a weakening of the

North Atlantic storm track. This decrease in storm track activity indicates a reduction of geopotential height variability in the SMHI-LENS (since storm tracks were identified in the standard deviation of high-pass filtered Z500, compare Figure 6). This decrease is in line with generally weaker geopotential height anomalies identified in the future simulation for the different regime patterns (compare Figure 3). Although no agreement on the response of the North Atlantic jet speed to external forcing was seen in different CMIP3 models in Woollings and Blackburn (2012), the weakening of storm track activity seen in this thesis assorts well with a weakening of the polar vortex and the jet stream in response to reduced Arctic sea ice in an atmospheric GCM described in Crasemann et al. (2017) and the decrease in extratropical cyclone intensity under increasing greenhouse gas concentrations in CMIP5 models in Catto et al. (2019). According to Francis and Vavrus (2015), a weaker jet stream is associated with a more meridional (i.e. wavier) flow character, which in turn could increase the frequency of extreme weather events due to persistent jet stream configurations. Other studies, however, project a strengthening for the wintertime North Atlantic storm track (Peings et al. 2018), which is not found in the SMHI-LENS with EC-Earth3, and the response is generally stronger in the current CMIP6 ensemble compared to its predecessor (Harvey et al. 2020; Priestley and Catto 2022).

6.2.1 Temperature changes

To evaluate future temperature changes, a general remark about global warming simulated by CMIP6 models needs to be made. A very recent study by Pan et al. (2023) recommends caution when interpreting Arctic climate change projected by CMIP6 models from the NEMO family. They found a common overestimation of AA in climate models that employ the NEMO ocean component family when investigating the response to SSP5-8.5 forcing, independent of the choice of atmosphere and sea ice models. They attribute the increased AA to stronger poleward ocean heat transport in this group of models compared to other CMIP6 members. However, taking into account that non-NEMO models are found to slightly underestimate AA in historical simulations, NEMO-family models may even perform better at projecting future Arctic climate change despite their overestimation of poleward ocean heat transport, since historical winter mixed-layer depth and sea ice extent are closer to observations (Pan et al. 2023). Nevertheless, keeping in mind that EC-Earth3 belongs to the NEMO-family climate models, the future Arctic warming projected by the SMHI-LENS is most probably rather at the upper end of the range of possible temperature responses, even within SSP5-8.5 simulations.

In general, temperatures are projected to rise in response to increased greenhouse gas emissions with the strongest increase in mean temperatures over the Arctic due to AA (as also seen in the future scenario ensemble mean in Figure 5b) and the future SAT changes simulated by the SMHI-LENS with EC-Earth3 are reported to be significant almost everywhere (Wyser et

al. 2021). Furthermore, there is strong evidence that the magnitude and probability of warm events are increasing under global warming (Walsh et al. 2020; Arias et al. 2021). This appears to be in contrast to the finding of a more narrow SAT distribution and less intense temperature extremes for most northerly latitudes as seen in Section 5 in this thesis. The increase in warm events in other studies, however, is rather an indication of the general background warming since extremes are often defined relative to the current climate (Walsh et al. 2020).

This motivates a look at additional statistical quantities, other than changes in the climatological average. Tamarin-Brodsky et al. (2020) investigated the response of temperature mean, variability, skewness, and extremes to strong RCP8.5 warming scenarios in CMIP5 models. They developed a theory explaining the dynamic generation of variance and skewness changes from changes in the mean temperature gradient, thereby also accounting for the response to global warming. In this framework, decreases in temperature variance are a direct consequence of the weakening of the mean temperature gradient due to reduced advection and temperature skewness is generated by linearly advecting non-uniform background temperature gradients.

As expected and in line with previous studies, both an increase in mean temperature and an additional decrease in temperature variance for northerly latitudes are observed (compare Figure 1c-d in Tamarin-Brodsky et al. 2020). This mean warming along with a decrease in SAT variability yields an explanation for an increase in warm events in a future climate (relative to the current climate), and at the same time allows for the decrease seen in temperature extremes for northerly latitudes in this thesis, which were computed relative to the future climate.

Also temperature skewness is projected to change under strong forcing scenarios. As a reminder: skewness measures the asymmetry between the positive and negative tails of a probability distribution, a symmetric (Gaussian) distribution consequentially has zero skewness. Skewness is positive (negative) if strong warm (cold) anomalies are more frequent. By the end of the century, Tamarin-Brodsky et al. (2020) showed negative wintertime SAT skewness changes over most of the Northern Hemisphere (compare their Figure 7f in the extended data). South of the 0 °C temperature line, a positive skewness shift was observed (Tamarin-Brodsky et al. 2020). The increase in variance in combination with the negative skewness change over northerly latitudes implies a stronger weakening of warm anomalies. This was suggested to be related to the effects of melting snow and sea ice, which is in line with the reasons discussed in Section 5 and the generally stronger reduction in warm extremes in Figure 15 compared to cold extremes. It is interesting to note that in their main manuscript, Tamarin-Brodsky et al. (2020) investigated changes at the 850 hPa level. They mention that their findings for the winter mean and variance apply to SAT as well, but that changes in winter skewness are of opposite sign for most northerly latitudes: positive at the 850 hPa level due to horizontal advection arguments and negative near the surface in relation with snow and sea-ice loss as described above.

The response to the strong warming scenario in the SAT regime composites (Fig. 10) was seen to be in line with the changes in the WR patterns. In the ERA5 reanalysis and the historical simulation, warm anomalies were seen to align with Z500 ridges, while cold conditions were rather co-located with troughs. This connection is seen to remain in the future, but the general weakening of Z500 anomalies under SSP5-8.5 forcing implies reduced Z500 gradients, thereby affecting the advection of warm and cold air by the large-scale circulation (Hurrell et al. 2003).

Cattiaux et al. (2013a) investigated the response of European temperatures in CMIP5 to the RCP8.5 scenario using the WR approach and found a moderate cooling effect in connection with a reduction in NAO– frequency, which is not seen in the SMHI-LENS as mentioned before. By separating the contributions of large-scale dynamics and regional processes to changes, they concluded that the projected European warming at the end of the 21st century is not primarily driven by circulation changes but rather by non-dynamical processes. Shifts in the Euro-Atlantic circulation are instead found to contribute to the inter-model spread. Again, their results were obtained by using pseudo-PCs and large spatial variability was actively suppressed.

Also the changes in temperature anomalies associated with blocking were investigated in several modelling studies and mostly attributed to changes in large-scale thermal advection (Kennedy et al. 2016; Woollings et al. 2018). Reduced amplitudes were found for both SAT and Z500 anomalies during Atlantic blocking conditions under strong RCP8.5 forcing applied to four different CMIP5 models (Masato et al. 2014). A weakening of the cooling associated with Atlantic winter blocking, especially over northeastern Europe, was also identified in Sillmann et al. (2011) in climate simulations with a coupled GCM. In fact, the decrease in both Z500 and SAT anomalies is in line with the changes seen during Atlantic Ridge regime conditions under the future SSP5-8.5 scenario simulation with the SMHI-LENS in this thesis (Figs. 4c and 10c) and also agrees with a general reduction in temperature variance as discussed before. Also during European blocking regimes, both the positive temperature anomalies over northern Europe and the cold anomalies over southern Europe have been reported to weaken under future warming experiments with an atmospheric model (Kennedy et al. 2016). Considering the general warming that is stronger over the Arctic Ocean and the European landmasses than over the Atlantic (see Fig. 5b) yields an explanation for this reduction: The anticyclonic large-scale circulation during these blocking episodes features warmer easterly winds to the south of the European ridge, while the westerlies to the north are warmed less by the subjacent ocean (Kennedy et al. 2016). In line with this, the Scandinavian Blocking regime in the SMHI-LENS SSP5-8.5 simulation is characterised by weaker SAT anomalies (Fig. 10b). A response that is not seen in the SMHI-LENS is a northeastward shift of the European winter blocking that is reported in Sillmann and Croci-Maspoli (2009) and Masato et al. (2014). If present, such a shift in blocking location could imply larger impacts (also in terms of temperature extremes) in regions that are less affected under the current climate (Woollings et al. 2018).

6.2.2 Changes in precipitation and storm tracks

In contrast to the reduction in SAT anomalies, precipitation anomalies were seen to strengthen in response to a strong warming scenario (Fig. 12). The general precipitation response to global warming is given by a mean increase that is, in general terms, consistent with the Clausius-Clapeyron relation (Held and Soden 2006; Catto et al. 2019; Walsh et al. 2020). Per °C of warming, an increase in atmospheric water vapour of 7% is expected, thereby effectively leading to more precipitable water in a warmer climate. Also intense precipitation associated with extratropical cyclones is projected to increase in these warmer and moister conditions (Catto et al. 2019). This is in line with the projected general increase in total precipitation for most regions in the SSP5-8.5 simulation ensemble mean (Fig. 5d). However, while future SAT changes in the SMHI-LENS were found to be significant, the precipitation response is much less robust and needs more ensemble members to be detected (Wyser et al. 2021). This has also been reported for other models (Deser et al. 2012).

Again, as discussed for SAT, not only the mean is subject to change, but also precipitation variability is altered in future climate simulations. In accordance with a wider precipitation distribution in the SMHI-LENS future simulation as seen in the increase in the probability of dry and wet extremes of historical magnitude (Figs. 16 and 17), precipitation variability is projected to increase in most regions in CMIP5 and other climate model large ensembles in response to RCP8.5 forcing (Pendergrass et al. 2017). This increase in precipitation variability is at least of the same order as the mean precipitation increase. However, it is weaker than the increase in moisture explained by the Clausius-Clapeyron relation and also than the increase in extreme precipitation, indicating that the effect of enhanced atmospheric moisture is to some extent attenuated by circulation changes (i.e. a weakened circulation related to enhanced mid-latitude stability) (Pendergrass et al. 2017).

Naturally, the modulation of the jet stream position and intensity during the different WRs is also reflected in the accompanying extratropical cyclone activity (Madonna et al. 2017). Pasquier et al. (2019) described the connection between these regime-dependent changes in the large-scale flow and the occurrence of atmospheric rivers and heavy precipitation events (compare also Yiou and Nogaj 2004). This link seems obvious considering the close connection between the North Atlantic jet stream and storm track and including the fact that most mid-latitude precipitation extremes are associated with storm tracks (Shaw et al. 2016). Moreover, this connection strongly suggests that North Atlantic jet stream and storm track responses to climate change are directly linked to changes in the Euro-Atlantic WRs.

The expected changes in response to global warming, however, are less straight-forward, as elucidated before in the discussion of the tug-of-war between the opposing effects of AA at the surface and upper-tropospheric warming in the tropics (Shaw et al. 2016; Catto et al. 2019;

Harvey et al. 2020). The actual response to enhanced greenhouse gas forcing will depend on the relative importance of these opposing influences. This is still under investigation, thereby also leading to a large spread in the modelled precipitation responses since the occurrence of wet extremes is favoured by strong storm track activity, while dry episodes are more connected to low activity (Lehmann and Coumou 2015) as was also seen in Chang et al. (2022), who estimated the impact of storm track changes on precipitation in CMIP5 and CMIP6 models. Regionally, they found substantial differences in the storm track changes projected by the models that can lead to significantly different regional precipitation impacts (Chang et al. 2022).

In line with this tug-of-war on storm track impacts, Yu et al. (2023) identified opposing influences of global ocean warming and sea-ice loss on precipitation. These opposing impacts are closely related to coincident changes in storm density and intensity, namely an equatorward shift of the North Atlantic storm track in response to sea-ice loss and a northeastern extension due to ocean warming. The future precipitation changes in the SMHI-LENS (Fig. 5d), which are dominated by a general wetting trend, are more in line with the response to future global ocean warming than to Arctic sea-ice loss in Yu et al. (2023). Also the projected drying in the Mediterranean region agrees with the response to increasing SSTs. Only the drying over the Atlantic south of Iceland appears to rather be attributed to Arctic sea-ice loss than increasing SSTs and is also present in the combined response to these opposing effects in Yu et al. (2023).

Connecting NAO and precipitation changes, Tsanis and Tapoglou (2019) found an increase in winter precipitation over northern and a decrease over southern Europe in accordance with more frequent extremely positive NAO phases. While this general precipitation trend was confirmed by McKenna and Maycock (2022), they described the NAO's role in precipitation projections to be small over northern Europe, whereas its role over southern Europe was seen to be substantial, thereby offering the potential for improved precipitation projections over this area by more reliably simulating changes in the NAO (McKenna and Maycock 2022). Unfortunately, this increase in NAO+ occurrence is hard to compare to the SMHI-LENS due to the misrepresentation of this regime. However, the more observation-consistent NAO− regime experiences a frequency decrease in the SMHI-LENS SSP5-8.5 simulation, which is in line with Tsanis and Tapoglou (2019) and McKenna and Maycock (2022).

A striking feature of the future SMHI-LENS simulation is a dry 'blob' south of Iceland seen in the changes of total precipitation anomalies relative to the historical simulation (Fig. 5d), which is in contrast to a general wintertime wetting trend at northerly latitudes. This dry 'blob' appears to also affect the changes in dry extremes for all regimes (Fig. 16) as described in Section 5. Also Zappa et al. (2013b), looking at RCP4.5 and 8.5 simulations in CMIP5 models (see their Fig. 2e), as well as Pendergrass et al. (2017), evaluating CMIP5 RCP8.5 projections (their Fig. 2), found a decrease in precipitation in this region, although less confined than the SMHI-LENS dry 'blob' region. As mentioned above, also Yu et al. (2023) found a drying

trend in this area in CMIP6 simulations (their Fig. 8) and pointed to Arctic sea-ice loss as the main driver. Another interesting aspect to consider could be changes in the Atlantic meridional overturning circulation (AMOC), since a large decline thereof has been connected to a reduction in precipitation south of Iceland in Bellomo et al. (2021).

Taking into account that most of the precipitation in the mid-latitudes is brought by extratropical cyclones along the storm tracks, this local drying trend could potentially be associated with changes in the intensity and location of the North Atlantic storm track. One could speculate that the general weakening and more zonal orientation of the storm track that is seen in the SSP5-8.5 scenario simulation at the end of the century (Fig. 6) is a potential contributor to the dry 'blob': A weaker and more zonally oriented North Atlantic storm track advects less precipitation from the southwest, instead more precipitation is brought from the west. When ascending over southern Greenland, these westerlies could favour orographic convection and increased precipitation over southeast Greenland, while reducing precipitation further downstream the North Atlantic storm track in the region south of Iceland. This is just a potential explanation of the observed dry 'blob' under the SSP5-8.5 scenario and requires further study to confirm.

Baker et al. (2019) also highlighted the role of horizontal resolution in modelling the precipitation associated with extratropical cyclones. Their study suggests that sufficient horizontal resolution is necessary to better resolve Greenland's topography and the precipitation associated with extratropical cyclones downstream of orography. Concretely, they found more of this precipitation over the Atlantic east of Greenland at higher resolutions (N512; corresponding to ca. 25 km grid spacing) compared with lower resolutions (N96; ca. 135 km) under historical forcing (see their Fig. 8). Under the SSP5-8.5 scenario, the difference in this region is less clear. Since the resolution of the atmospheric component of the SMHI-LENS is closer to the lower resolution simulation, this could be an additional factor to take into account when analysing the precipitation response downstream of orography.

All in all, there still remains considerable uncertainty about future climate change in general and the response of WRs in particular. The results obtained with the SMHI-LENS in this thesis are seen to be in line with some of the previous studies, especially the general changes in SAT and precipitation agree with the scientific consensus (Arias et al. 2021; Wyser et al. 2021). At the same time, the future of the Euro-Atlantic WRs remains particularly unclear and difficult to project. Since the use of pseudo-PCs, on the one hand, assumes time-invariance of the regime patterns, while, on the other hand, the agreement with observational regimes in this thesis was notably affected by the use of the respective dataset's PCs, the scientific community appears to always be prompted to make a compromise. Nevertheless, the general changes in the SMHI-LENS future simulation are seen to also apply to the different WRs, thereby allowing for confidence in these results and promoting the (non-pseudo-PC) approach used in this thesis.

7 Summary and Conclusions

In this thesis, weather regime clustering was applied to reanalysis and climate model ensemble data from the Swedish Meteorological and Hydrological Institute Large Ensemble (SMHI-LENS) with EC-Earth3 to identify the changes in the dominant Euro-Atlantic Weather regimes (WRs) in response to a strong global warming scenario. The emerging regime patterns were compared between the different datasets before assessing the impact of the different WRs on tropospheric weather as seen in near-surface temperature SAT and precipitation as well as the effect on extreme events with respect to those variables.

Using the ERA5 reanalysis, the known wintertime Euro-Atlantic WRs were identified in the geopotential height field. These WRs were seen to bring different SAT and precipitation anomaly patterns that agree with the anomalies described in the literature. Despite considerable biases, especially in the North Atlantic sector, the historical SMHI-LENS simulation was able to reproduce an atmospheric circulation system with four distinguishable WRs. The quality of the individual regimes' representations, however, differed. While Scandinavian Blocking was represented very well, the ensemble struggled most at reproducing the positive NAO phase. In accordance with the differences in the simulated compared to the observed WRs, the modelled SAT and total precipitation patterns were similar for all but the NAO+ regime. These differences between ERA5 and the historical SMHI-LENS results are likely attributable to the North Atlantic biases in SAT and SST, as well as a bias in the North Atlantic jet stream. Nevertheless, considering these significant biases in the North Atlantic region and the model's resolution of around 80 km, the SMHI-LENS proved to be able to reproduce three out of four weather regimes surprisingly well.

The response to the SSP5-8.5 forcing scenario was investigated by looking at the emerging regime patterns, their associated SAT and precipitation composites as well as the changes in extreme weather. Under the strong global warming simulation, the geopotential height anomalies associated with the different WRs remained very similar to the historical simulation. However, the anomalies' magnitude decreased for most regimes, thereby effectively reducing the Z500 gradient. Only the NAO- regime showed an increased Z500 gradient.

Likewise, the general SAT and precipitation patterns were seen to be unchanged by the SSP5-8.5 forcing. Nevertheless, while the magnitude of the SAT anomalies and extremes decreased over northerly latitudes, precipitation anomalies and extreme events were seen to mostly strengthen for all WR. As discussed in Section 6, the SAT changes, corresponding to a narrowing of the SAT distribution, can be understood in terms of a strongly elevated mean temperature at the end of the century that is accompanied by a decrease in temperature variance. The precipitation changes, on the other hand, given by a widening distribution, were postulated to agree with enhanced atmospheric moisture and increased variability following the Clausius-

Clapeyron relationship. Regional differences in the changes in the probability of extreme events between the individual WRs were seen to be in line with the composited mean SAT and precipitation patterns.

The primary objectives of this thesis were to investigate the future changes in the dominant Euro-Atlantic WRs in response to a strong global warming scenario and to assess the accompanying temperature and precipitation changes. The SMHI-LENS with EC-Earth3 was seen to be a useful tool in examining this response by giving robust results for the historical and the future simulation, respectively. Generally, the WRs in the SMHI-LENS showed a similar spatial pattern under the SSP5-8.5 scenario compared to the historical simulation albeit with reduced magnitude for all regimes but the NAO–, and the SAT and precipitation changes accompanying the individual WRs were seen to be in line with the general shifts expected under global warming. Nevertheless, many uncertainties remain and motivate further investigation of this topic. Especially the representation of the historical WR patterns in the SMHI-LENS was identified as a limiting factor. Considering their spatial agreement with the future regime patterns, a more realistic representation would very likely also improve the WR projections. But already with the shortcomings listed before, the SMHI-LENS was able to give insights into possible future changes, with these shifts being within the range discussed in the literature.

Using large ensembles like the SMHI-LENS offers many possibilities for future studies. An interesting extension of the work conducted in this thesis could be to compare the magnitude of the forced response seen in the SMHI-LENS future simulation with the magnitude of the natural variability in the ensemble. This could help to assess and interpret the seen response in the different variables in light of their present-day and future internal variability.

Also studying the impact of the El Niño-Southern Oscillation (ENSO) or the Madden-Julian Oscillation (MJO) by only sampling within a certain ENSO state or MJO phase could be a use case for the SMHI-LENS. Since interaction between these oscillations and the Euro-Atlantic WRs, especially the NAO, has been described in previous studies (e.g. Cassou 2008; Fereday et al. 2020), this could further support the disentangling of the complex interplay that forms the mid-latitude wintertime circulation.

Finally, repeating the analysis in this thesis with one or more large ensembles performed with different models would help to review the results obtained with the SMHI-LENS.

References

Arias, P., N. Bellouin, E. Coppola, R. Jones, et al. (2021). "Technical summary". In: *Climate change 2021: The physical science basis. Contribution of working group I to the sixth assessment report of the intergovernmental panel on climate change.* Ed. by V. Masson-Delmotte, P. Zhai, A. Pirani, S. Connors, et al. Cambridge, United Kingdom and New York, NY, USA: Cambridge University Press, pp. 33–144. DOI: 10.1017/9781009157896.002.

Arthur, D. and S. Vassilvitskii (2006). *k-means++: The advantages of careful seeding.* Technical report 2006-13. Stanford / Stanford InfoLab. URL: http://ilpubs.stanford.edu:8090/778/ (visited on 03/01/2023).

Bacer, S., F. Jomaa, J. Beaumet, H. Gallée, et al. (2022). "Impact of climate change on wintertime European atmospheric blocking". In: *Weather and Climate Dynamics* 3.1, pp. 377–389. DOI: 10.5194/wcd-3-377-2022.

Baker, A. J., R. Schiemann, K. I. Hodges, M.-E. Demory, et al. (2019). "Enhanced Climate Change Response of Wintertime North Atlantic Circulation, Cyclonic Activity, and Precipitation in a 25-km-Resolution Global Atmospheric Model". In: *Journal of Climate* 32.22, pp. 7763–7781. DOI: 10.1175/JCLI-D-19-0054.1.

Balsari, S., C. Dresser, and J. Leaning (2020). "Climate Change, Migration, and Civil Strife". In: *Current Environmental Health Reports* 7.4, pp. 404–414. DOI: 10.1007/s40572-020-00291-4.

Barnes, E. A. and L. Polvani (2013). "Response of the Midlatitude Jets, and of Their Variability, to Increased Greenhouse Gases in the CMIP5 Models". In: *Journal of Climate* 26.18, pp. 7117–7135. DOI: 10.1175/JCLI-D-12-00536.1.

Barriopedro, D., R. García-Herrera, A. R. Lupo, and E. Hernández (2006). "A Climatology of Northern Hemisphere Blocking". In: *Journal of Climate* 19.6, pp. 1042–1063. DOI: 10.1175/JCLI3678.1.

Baur, F., P. Hess, and H. Nagel (1944). "Kalender der Grosswetterlagen Europas 1881–1939". In: *Bad Homburg* 35.

Bellomo, K., M. Angeloni, S. Corti, and J. von Hardenberg (2021). "Future climate change shaped by inter-model differences in Atlantic meridional overturning circulation response". In: *Nature Communications* 12.1, p. 3659. DOI: 10.1038/s41467-021-24015-w.

Blackmon, M. L. (1976). "A climatological spectral study of the 500 mb geopotential height of the Northern Hemisphere". In: *Journal of the Atmospheric Sciences* 33.8, pp. 1607–1623.

Cassou, C. (2008). "Intraseasonal interaction between the Madden–Julian Oscillation and the North Atlantic Oscillation". In: *Nature* 455.7212, pp. 523–527. DOI: 10.1038/nature07286.

Cassou, C., L. Terray, and A. S. Phillips (2005). "Tropical Atlantic Influence on European Heat Waves". In: *Journal of Climate* 18.15, pp. 2805–2811. DOI: 10.1175/JCLI3506.1.

Cattiaux, J., H. Douville, and Y. Peings (2013a). "European temperatures in CMIP5: origins of present-day biases and future uncertainties". In: *Climate Dynamics* 41.11, pp. 2889–2907. DOI: 10.1007/s00382-013-1731-y.

Cattiaux, J., B. Quesada, A. Arakélian, F. Codron, et al. (2013b). "North-Atlantic dynamics and European temperature extremes in the IPSL model: sensitivity to atmospheric resolution". In: *Climate Dynamics* 40.9, pp. 2293–2310. DOI: 10.1007/s00382-012-1529-3.

Catto, J. L., D. Ackerley, J. F. Booth, A. J. Champion, et al. (2019). "The Future of Midlatitude Cyclones". In: *Current Climate Change Reports* 5.4, pp. 407–420. DOI: 10.1007/s40641-019-00149-4.

Chang, E. K.-M., A. M.-W. Yau, and R. Zhang (2022). "Finding Storm Track Activity Metrics That Are Highly Correlated with Weather Impacts. Part II: Estimating Precipitation Change Associated with Projected Storm Track Change over Europe". In: *Journal of Climate* 35.8, pp. 2423–2440. DOI: 10.1175/JCLI-D-21-0259.1.

Chiang, M. M.-T. and B. Mirkin (2007). "Experiments for the Number of Clusters in K-Means". In: *Progress in Artificial Intelligence*. Ed. by J. Neves, M. F. Santos, and J. M. Machado. Lecture Notes in Computer Science. Berlin, Heidelberg: Springer, pp. 395–405. DOI: 10.1007/978-3-540-77002-2_33.

Chu, C., X.-Q. Yang, X. Ren, and T. Zhou (2013). "Response of Northern Hemisphere storm tracks to Indian-western Pacific Ocean warming in atmospheric general circulation models". In: *Climate Dynamics* 40.5, pp. 1057–1070. DOI: 10.1007/s00382-013-1687-y.

Coelho, C. a. S., C. a. T. Ferro, D. B. Stephenson, and D. J. Steinskog (2008). "Methods for Exploring Spatial and Temporal Variability of Extreme Events in Climate Data". In: *Journal of Climate* 21.10, pp. 2072–2092. DOI: 10.1175/2007JCLI1781.1.

Cortesi, N., V. Torralba, L. Lledó, A. Manrique-Suñén, et al. (2021). "Yearly evolution of Euro-Atlantic weather regimes and of their sub-seasonal predictability". In: *Climate Dynamics* 56.11, pp. 3933–3964. DOI: 10.1007/s00382-021-05679-y.

Crasemann, B., D. Handorf, R. Jaiser, K. Dethloff, et al. (2017). "Can preferred atmospheric circulation patterns over the North-Atlantic-Eurasian region be associated with arctic sea ice loss?" In: *Polar Science* 14, pp. 9–20. DOI: 10.1016/j.polar.2017.09.002.

Danabasoglu, G., S. G. Yeager, D. Bailey, E. Behrens, et al. (2014). "North Atlantic simulations in Coordinated Ocean-ice Reference Experiments phase II (CORE-II). Part I: Mean states". In: *Ocean Modelling* 73, pp. 76–107. DOI: 10.1016/j.ocemod.2013.10.005.

Davini, P. and F. D'Andrea (2020). "From CMIP3 to CMIP6: Northern Hemisphere Atmospheric Blocking Simulation in Present and Future Climate". In: *Journal of Climate* 33.23, pp. 10021–10038. DOI: 10.1175/JCLI-D-19-0862.1.

Dawson, A., T. N. Palmer, and S. Corti (2012). "Simulating regime structures in weather and climate prediction models". In: *Geophysical Research Letters* 39.21. DOI: 10.1029/2012GL053284.

Dawson, A. and T. N. Palmer (2015). "Simulating weather regimes: impact of model resolution and stochastic parameterization". In: *Climate Dynamics* 44.7, pp. 2177–2193. DOI: 10.1007/s00382-014-2238-x.

de Vries, H., T. Woollings, J. Anstey, R. J. Haarsma, and W. Hazeleger (2013). "Atmospheric blocking and its relation to jet changes in a future climate". In: *Climate Dynamics* 41.9, pp. 2643–2654. DOI: 10.1007/s00382-013-1699-7.

Delgado-Torres, C., D. Verfaillie, E. Mohino, and M. G. Donat (2022). "Representation and Annual to Decadal Predictability of Euro-Atlantic Weather Regimes in the CMIP6 Version of the EC-Earth Coupled Climate Model". In: *Journal of Geophysical Research: Atmospheres* 127.14, e2022JD036673. DOI: 10.1029/2022JD036673.

Deser, C., A. S. Phillips, I. R. Simpson, N. Rosenbloom, et al. (2020). "Isolating the Evolving Contributions of Anthropogenic Aerosols and Greenhouse Gases: A New CESM1 Large Ensemble Community Resource". In: *Journal of Climate* 33.18, pp. 7835–7858. DOI: 10.1175/JCLI-D-20-0123.1.

Deser, C., A. Phillips, V. Bourdette, and H. Teng (2012). "Uncertainty in climate change projections: the role of internal variability". In: *Climate Dynamics* 38.3, pp. 527–546. DOI: 10.1007/s00382-010-0977-x.

Dorrington, J. and K. J. Strommen (2020). "Jet Speed Variability Obscures Euro-Atlantic Regime Structure". In: *Geophysical Research Letters* 47.15, e2020GL087907. DOI: 10.1029/2020GL087907.

Dorrington, J., K. Strommen, and F. Fabiano (2022). "Quantifying climate model representation of the wintertime Euro-Atlantic circulation using geopotential-jet regimes". In: *Weather and Climate Dynamics* 3.2, pp. 505–533. DOI: `10.5194/wcd-3-505-2022`.

Döscher, R., M. Acosta, A. Alessandri, P. Anthoni, et al. (2021). "The EC-Earth3 Earth System Model for the Climate Model Intercomparison Project 6". In: *Geoscientific Model Development Discussions* 1, pp. 2973–3020.

Eyring, V., S. Bony, G. A. Meehl, C. A. Senior, et al. (2016). "Overview of the Coupled Model Intercomparison Project Phase 6 (CMIP6) experimental design and organization". In: *Geoscientific Model Development* 9.5, pp. 1937–1958. DOI: `10.5194/gmd-9-1937-2016`.

Fabiano, F., H. M. Christensen, K. Strommen, P. Athanasiadis, et al. (2020). "Euro-Atlantic weather Regimes in the PRIMAVERA coupled climate simulations: impact of resolution and mean state biases on model performance". In: *Climate Dynamics* 54.11, pp. 5031–5048. DOI: `10.1007/s00382-020-05271-w`.

Fabiano, F., V. L. Meccia, P. Davini, P. Ghinassi, and S. Corti (2021). "A regime view of future atmospheric circulation changes in northern mid-latitudes". In: *Weather and Climate Dynamics* 2.1, pp. 163–180. DOI: `10.5194/wcd-2-163-2021`.

Fereday, D. R., R. Chadwick, J. R. Knight, and A. A. Scaife (2020). "Tropical Rainfall Linked to Stronger Future ENSO-NAO Teleconnection in CMIP5 Models". In: *Geophysical Research Letters* 47.22, e2020GL088664. DOI: `10.1029/2020GL088664`.

Ferranti, L., S. Corti, and M. Janousek (2015). "Flow-dependent verification of the ECMWF ensemble over the Euro-Atlantic sector". In: *Quarterly Journal of the Royal Meteorological Society* 141.688, pp. 916–924. DOI: `10.1002/qj.2411`.

Field, C. B., V. Barros, T. F. Stocker, and Q. Dahe (2012). *Managing the risks of extreme events and disasters to advance climate change adaptation: special report of the intergovernmental panel on climate change.* Cambridge University Press.

Francis, J. A. and S. J. Vavrus (2015). "Evidence for a wavier jet stream in response to rapid Arctic warming". In: *Environmental Research Letters* 10.1, p. 014005. DOI: `10.1088/1748-9326/10/1/014005`.

Hannachi, Abdel., D. M. Straus, C. L. E. Franzke, S. Corti, and T. Woollings (2017). "Low-frequency nonlinearity and regime behavior in the Northern Hemisphere extratropical atmosphere". In: *Reviews of Geophysics* 55.1, pp. 199–234. DOI: `10.1002/2015RG000509`.

Harvey, B. J., P. Cook, L. C. Shaffrey, and R. Schiemann (2020). "The Response of the Northern Hemisphere Storm Tracks and Jet Streams to Climate Change in the CMIP3, CMIP5, and CMIP6 Climate Models". In: *Journal of Geophysical Research: Atmospheres* 125.23, e2020JD032701. DOI: `10.1029/2020JD032701`.

Heikkilä, U., A. Sandvik, and A. Sorteberg (2011). "Dynamical downscaling of ERA-40 in complex terrain using the WRF regional climate model". In: *Climate Dynamics* 37.7, pp. 1551–1564. DOI: `10.1007/s00382-010-0928-6`.

Held, I. M. and B. J. Soden (2006). "Robust Responses of the Hydrological Cycle to Global Warming". In: *Journal of Climate* 19.21, pp. 5686–5699. DOI: `10.1175/JCLI3990.1`.

Hersbach, H., B. Bell, P. Berrisford, S. Hirahara, et al. (2020). "The ERA5 global reanalysis". In: *Quarterly Journal of the Royal Meteorological Society* 146.730, pp. 1999–2049. DOI: `10.1002/qj.3803`.

Hertig, E. and J. Jacobeit (2014). "Variability of weather regimes in the North Atlantic-European area: past and future". In: *Atmospheric Science Letters* 15.4, pp. 314–320. DOI: `10.1002/asl2.505`.

Hurrell, J. W., Y. Kushnir, G. Ottersen, and M. Visbeck (2003). "An overview of the North Atlantic oscillation". In: *Geophysical Monograph-American Geophysical Union* 134, pp. 1–36. DOI: `10.1029/134GM01`.

Ikotun, A. M., A. E. Ezugwu, L. Abualigah, B. Abuhaija, and J. Heming (2023). "K-means clustering algorithms: A comprehensive review, variants analysis, and advances in the era of big data". In: *Information Sciences* 622, pp. 178–210. DOI: 10.1016/j.ins.2022.11.139.

Jensen, C., T. Mahavadi, N. H. Schade, I. Hache, and T. Kruschke (2022). "Negative Storm Surges in the Elbe Estuary—Large-Scale Meteorological Conditions and Future Climate Change". In: *Atmosphere* 13.10, p. 1634. DOI: 10.3390/atmos13101634.

John, A., H. Douville, A. Ribes, and P. Yiou (2022). "Quantifying CMIP6 model uncertainties in extreme precipitation projections". In: *Weather and Climate Extremes* 36, p. 100435. DOI: 10.1016/j.wace.2022.100435.

Kautz, L.-A., O. Martius, S. Pfahl, J. G. Pinto, et al. (2022). "Atmospheric blocking and weather extremes over the Euro-Atlantic sector – a review". In: *Weather and Climate Dynamics* 3.1, pp. 305–336. DOI: 10.5194/wcd-3-305-2022.

Keller, L. M., K. J. Maloney, M. A. Lazzara, D. E. Mikolajczyk, and S. D. Battista (2022). "An Investigation of Extreme Cold Events at the South Pole". In: *Journal of Climate* 35.6, pp. 1761–1772. DOI: 10.1175/JCLI-D-21-0404.1.

Kennedy, D., T. Parker, T. Woollings, B. Harvey, and L. Shaffrey (2016). "The response of high-impact blocking weather systems to climate change". In: *Geophysical Research Letters* 43.13, pp. 7250–7258. DOI: 10.1002/2016GL069725.

Kidson, J. W. and M. R. Sinclair (1995). "The Influence of Persistent Anomalies on Southern Hemisphere Storm Tracks". In: *Journal of Climate* 8.8, pp. 1938–1950. DOI: 10.1175/1520-0442(1995)008<1938:TIOPAO>2.0.CO;2.

Kim, K.-H., E. Kabir, and S. Ara Jahan (2014). "A Review of the Consequences of Global Climate Change on Human Health". In: *Journal of Environmental Science and Health, Part C* 32.3, pp. 299–318. DOI: 10.1080/10590501.2014.941279.

Koenigk, T., L. Brodeau, R. G. Graversen, J. Karlsson, et al. (2013). "Arctic climate change in 21st century CMIP5 simulations with EC-Earth". In: *Climate Dynamics* 40.11, pp. 2719–2743. DOI: 10.1007/s00382-012-1505-y.

Lau, N.-C. (1988). "Variability of the Observed Midlatitude Storm Tracks in Relation to Low-Frequency Changes in the Circulation Pattern". In: *Journal of the Atmospheric Sciences* 45.19, pp. 2718–2743. DOI: 10.1175/1520-0469(1988)045<2718:VOTOMS>2.0.CO;2.

Lehmann, J. and D. Coumou (2015). "The influence of mid-latitude storm tracks on hot, cold, dry and wet extremes". In: *Scientific Reports* 5.1, p. 17491. DOI: 10.1038/srep17491.

Lehner, F., C. Deser, N. Maher, J. Marotzke, et al. (2020). "Partitioning climate projection uncertainty with multiple large ensembles and CMIP5/6". In: *Earth System Dynamics* 11.2, pp. 491–508. DOI: 10.5194/esd-11-491-2020.

Lenderink, G. and E. van Meijgaard (2008). "Increase in hourly precipitation extremes beyond expectations from temperature changes". In: *Nature Geoscience* 1.8, pp. 511–514. DOI: 10.1038/ngeo262.

Levick, R. B. M. (1949). "Fifty years of English weather". In: *Weather* 4.7, pp. 206–211.

Lloyd, S. (1982). "Least squares quantization in PCM". In: *IEEE Transactions on Information Theory* 28.2, pp. 129–137. DOI: 10.1109/TIT.1982.1056489.

Löfverström, M. (2020). "A dynamic link between high-intensity precipitation events in southwestern North America and Europe at the Last Glacial Maximum". In: *Earth and Planetary Science Letters* 534, p. 116081. DOI: 10.1016/j.epsl.2020.116081.

Lorenz, E. N. (1963). "Deterministic Nonperiodic Flow". In: *Journal of the Atmospheric Sciences* 20.2, pp. 130–141. DOI: `10.1175/1520-0469(1963)020<0130:DNF>2.0.CO;2`.

MacQueen, J. (1967). "Some methods for classification and analysis of multivariate observations". In: *Proceedings of the Fifth Berkeley Symposium on Mathematical Statistics and Probability, Volume 1: Statistics* 5.1, pp. 281–298.

Madonna, E., C. Li, C. M. Grams, and T. Woollings (2017). "The link between eddy-driven jet variability and weather regimes in the North Atlantic-European sector". In: *Quarterly Journal of the Royal Meteorological Society* 143.708, pp. 2960–2972. DOI: `10.1002/qj.3155`.

Maher, N., S. Milinski, and R. Ludwig (2021). "Large ensemble climate model simulations: Introduction, overview, and future prospects for utilising multiple types of large ensemble". In: *Earth System Dynamics* 12, pp. 401–418. DOI: `10.5194/esd-12-401-2021`.

Martinez-Villalobos, C. and J. D. Neelin (2019). "Why Do Precipitation Intensities Tend to Follow Gamma Distributions?" In: *Journal of the Atmospheric Sciences* 76.11, pp. 3611–3631. DOI: `10.1175/JAS-D-18-0343.1`.

Masato, G., T. Woollings, and B. J. Hoskins (2014). "Structure and impact of atmospheric blocking over the Euro-Atlantic region in present-day and future simulations". In: *Geophysical Research Letters* 41.3, pp. 1051–1058. DOI: `10.1002/2013GL058570`.

McCrystall, M. R., J. Stroeve, M. Serreze, B. C. Forbes, and J. A. Screen (2021). "New climate models reveal faster and larger increases in Arctic precipitation than previously projected". In: *Nature Communications* 12.1, p. 6765. DOI: `10.1038/s41467-021-27031-y`.

McKenna, C. M. and A. C. Maycock (2022). "The Role of the North Atlantic Oscillation for Projections of Winter Mean Precipitation in Europe". In: *Geophysical Research Letters* 49.19, e2022GL099083. DOI: `10.1029/2022GL099083`. (Visited on 04/07/2023).

Meier, W. N., D. Perovich, S. Farrell, C. Haas, et al. (2021). "NOAA Arctic Report Card 2021: Sea Ice". In: DOI: `10.25923/Y2WD-FN85`.

Michel, C., G. Rivière, L. Terray, and B. Joly (2012). "The dynamical link between surface cyclones, upper-tropospheric Rossby wave breaking and the life cycle of the Scandinavian blocking". In: *Geophysical Research Letters* 39.10. DOI: `10.1029/2012GL051682`.

Michelangeli, P.-A., R. Vautard, and B. Legras (1995). "Weather Regimes: Recurrence and Quasi Stationarity". In: *Journal of the Atmospheric Sciences* 52.8, pp. 1237–1256. DOI: `10.1175/1520-0469(1995)052<1237:WRRAQS>2.0.CO;2`.

Mittermeier, M., M. Weigert, D. Rügamer, H. Küchenhoff, and R. Ludwig (2022). "A deep learning based classification of atmospheric circulation types over Europe: projection of future changes in a CMIP6 large ensemble". In: *Environmental Research Letters* 17.8, p. 084021. DOI: `10.1088/1748-9326/ac8068`.

Nabizadeh, E., S. W. Lubis, and P. Hassanzadeh (2021). "The 3D Structure of Northern Hemisphere Blocking Events: Climatology, Role of Moisture, and Response to Climate Change". In: *Journal of Climate* 34.24, pp. 9837–9860. DOI: `10.1175/JCLI-D-21-0141.1`.

O'Neill, B. C., C. Tebaldi, D. P. van Vuuren, V. Eyring, et al. (2016). "The Scenario Model Intercomparison Project (ScenarioMIP) for CMIP6". In: *Geoscientific Model Development* 9.9, pp. 3461–3482. DOI: `10.5194/gmd-9-3461-2016`.

Palmer, T. N. (1999). "A Nonlinear Dynamical Perspective on Climate Prediction". In: *Journal of Climate* 12.2, pp. 575–591. DOI: `10.1175/1520-0442(1999)012<0575:ANDPOC>2.0.CO;2`.

Pan, R., Q. Shu, Q. Wang, S. Wang, et al. (2023). "Future Arctic Climate Change in CMIP6 Strikingly Intensified by NEMO-Family Climate Models". In: *Geophysical Research Letters* 50.4, e2022GL102077. DOI: 10.1029/2022GL102077.

Pasquier, J. T., S. Pfahl, and C. M. Grams (2019). "Modulation of Atmospheric River Occurrence and Associated Precipitation Extremes in the North Atlantic Region by European Weather Regimes". In: *Geophysical Research Letters* 46.2, pp. 1014–1023. DOI: 10.1029/2018GL081194.

Peings, Y., J. Cattiaux, S. Vavrus, and G. Magnusdottir (2017). "Late Twenty-First-Century Changes in the Midlatitude Atmospheric Circulation in the CESM Large Ensemble". In: *Journal of Climate* 30.15, pp. 5943–5960. DOI: 10.1175/JCLI-D-16-0340.1.

Peings, Y., J. Cattiaux, S. J. Vavrus, and G. Magnusdottir (2018). "Projected squeezing of the wintertime North-Atlantic jet". In: *Environmental Research Letters* 13.7, p. 074016. DOI: 10.1088/1748-9326/aacc79.

Pendergrass, A. G., R. Knutti, F. Lehner, C. Deser, and B. M. Sanderson (2017). "Precipitation variability increases in a warmer climate". In: *Scientific Reports* 7.1, p. 17966. DOI: 10.1038/s41598-017-17966-y.

Pendergrass, A. G., K. A. Reed, and B. Medeiros (2016). "The link between extreme precipitation and convective organization in a warming climate: Global radiative-convective equilibrium simulations". In: *Geophysical Research Letters* 43.21, pp. 11, 445–11, 452. DOI: 10.1002/2016GL071285.

Pfahl, S., P. A. O'Gorman, and E. M. Fischer (2017). "Understanding the regional pattern of projected future changes in extreme precipitation". In: *Nature Climate Change* 7.6, pp. 423–427. DOI: 10.1038/nclimate3287.

Piazza, M., L. Terray, J. Boé, E. Maisonnave, and E. Sanchez-Gomez (2016). "Influence of small-scale North Atlantic sea surface temperature patterns on the marine boundary layer and free troposphere: a study using the atmospheric ARPEGE model". In: *Climate Dynamics* 46.5, pp. 1699–1717. DOI: 10.1007/s00382-015-2669-z.

Pinto, J. G. and C. C. Raible (2012). "Past and recent changes in the North Atlantic oscillation". In: *WIREs Climate Change* 3.1, pp. 79–90. DOI: 10.1002/wcc.150.

Pinto, J. G., S. Zacharias, A. H. Fink, G. C. Leckebusch, and U. Ulbrich (2009). "Factors contributing to the development of extreme North Atlantic cyclones and their relationship with the NAO". In: *Climate Dynamics* 32.5, pp. 711–737. DOI: 10.1007/s00382-008-0396-4.

Plaut, G. and E. Simonnet (2001). "Large-scale circulation classification, weather regimes, and local climate over France, the Alps and Western Europe". In: *Climate Research* 17.3, pp. 303–324. DOI: 10.3354/cr017303.

Previdi, M., K. L. Smith, and L. M. Polvani (2021). "Arctic amplification of climate change: a review of underlying mechanisms". In: *Environmental Research Letters* 16.9, p. 093003. DOI: 10.1088/1748-9326/ac1c29.

Priestley, M. D. K. and J. L. Catto (2022). "Future changes in the extratropical storm tracks and cyclone intensity, wind speed, and structure". In: *Weather and Climate Dynamics* 3.1, pp. 337–360. DOI: 10.5194/wcd-3-337-2022.

Reinhold, B. B. and R. T. Pierrehumbert (1982). "Dynamics of Weather Regimes: Quasi-Stationary Waves and Blocking". In: *Monthly Weather Review* 110.9, pp. 1105–1145. DOI: 10.1175/1520-0493(1982)110<1105:DOWRQS>2.0.CO;2.

Rex, D. F. (1951). "The Effect of Atlantic Blocking Action upon European Climate". In: *Tellus* 3.2, pp. 100–112. DOI: 10.1111/j.2153-3490.1951.tb00784.x.

Roberts, M. J., A. Baker, E. W. Blockley, D. Calvert, et al. (2019). "Description of the resolution hierarchy of the global coupled HadGEM3-GC3.1 model as used in CMIP6 HighResMIP experiments". In: *Geoscientific Model Development* 12.12, pp. 4999–5028. DOI: 10.5194/gmd-12-4999-2019.

Sawyer, J. S. (1970). "Observational characteristics of atmospheric fluctuations with a time scale of a month". In: *Quarterly Journal of the Royal Meteorological Society* 96.410, pp. 610–625. DOI: 10.1002/qj.49709641005.

Scaife, A. A., D. Copsey, C. Gordon, C. Harris, et al. (2011). "Improved Atlantic winter blocking in a climate model". In: *Geophysical Research Letters* 38.23. DOI: 10.1029/2011GL049573.

Schaeffer, R., A. S. Szklo, A. F. Pereira de Lucena, B. S. Moreira Cesar Borba, et al. (2012). "Energy sector vulnerability to climate change: A review". In: *Energy* 38.1, pp. 1–12. DOI: 10.1016/j.energy.2011.11.056.

Schiemann, R., M.-E. Demory, L. C. Shaffrey, J. Strachan, et al. (2017). "The Resolution Sensitivity of Northern Hemisphere Blocking in Four 25-km Atmospheric Global Circulation Models". In: *Journal of Climate* 30.1, pp. 337–358. DOI: 10.1175/JCLI-D-16-0100.1.

Shaw, T. A., M. Baldwin, E. A. Barnes, R. Caballero, et al. (2016). "Storm track processes and the opposing influences of climate change". In: *Nature Geoscience* 9.9, pp. 656–664. DOI: 10.1038/ngeo2783.

Sickmöller, M., R. Blender, and K. Fraedrich (2000). "Observed winter cyclone tracks in the northern hemisphere in re-analysed ECMWF data". In: *Quarterly Journal of the Royal Meteorological Society* 126.563, pp. 591–620. DOI: 10.1002/qj.49712656311.

Sillmann, J. and M. Croci-Maspoli (2009). "Present and future atmospheric blocking and its impact on European mean and extreme climate". In: *Geophysical Research Letters* 36.10. DOI: 10.1029/2009GL038259.

Sillmann, J., M. Croci-Maspoli, M. Kallache, and R. W. Katz (2011). "Extreme Cold Winter Temperatures in Europe under the Influence of North Atlantic Atmospheric Blocking". In: *Journal of Climate* 24.22, pp. 5899–5913. DOI: 10.1175/2011JCLI4075.1.

Strommen, K., I. Mavilia, S. Corti, M. Matsueda, et al. (2019). "The Sensitivity of Euro-Atlantic Regimes to Model Horizontal Resolution". In: *Geophysical Research Letters* 46.13, pp. 7810–7818. DOI: 10.1029/2019GL082843.

Tamarin-Brodsky, T., K. Hodges, B. J. Hoskins, and T. G. Shepherd (2020). "Changes in Northern Hemisphere temperature variability shaped by regional warming patterns". In: *Nature Geoscience* 13.6, pp. 414–421. DOI: 10.1038/s41561-020-0576-3.

Tol, R. S. J. (2018). "The Economic Impacts of Climate Change". In: *Review of Environmental Economics and Policy* 12.1, pp. 4–25. DOI: 10.1093/reep/rex027.

Trigo, I. F., T. D. Davies, and G. R. Bigg (2000). "Decline in Mediterranean rainfall caused by weakening of Mediterranean cyclones". In: *Geophysical Research Letters* 27.18, pp. 2913–2916. DOI: 10.1029/2000GL011526.

Trigo, I. F. (2006). "Climatology and interannual variability of storm-tracks in the Euro-Atlantic sector: a comparison between ERA-40 and NCEP/NCAR reanalyses". In: *Climate Dynamics* 26.2, pp. 127–143. DOI: 10.1007/s00382-005-0065-9.

Tsanis, I. and E. Tapoglou (2019). "Winter North Atlantic Oscillation impact on European precipitation and drought under climate change". In: *Theoretical and Applied Climatology* 135.1, pp. 323–330. DOI: 10.1007/s00704-018-2379-7.

Ullmann, A., B. Fontaine, and P. Roucou (2014). "Euro-Atlantic weather regimes and Mediterranean rainfall patterns: present-day variability and expected changes under CMIP5 projections". In: *International Journal of Climatology* 34.8, pp. 2634–2650. DOI: 10.1002/joc.3864.

Vrac, M., P. Vaittinada Ayar, and P. Yiou (2014). "Trends and variability of seasonal weather regimes". In: *International Journal of Climatology* 34.2, pp. 472–480. DOI: 10.1002/joc.3700.

Walsh, J. E., T. J. Ballinger, E. S. Euskirchen, E. Hanna, et al. (2020). "Extreme weather and climate events in northern areas: A review". In: *Earth-Science Reviews* 209, p. 103324. DOI: 10.1016/j.earscirev.2020.103324.

Wei, T., Q. Yan, W. Qi, M. Ding, and C. Wang (2020). "Projections of Arctic sea ice conditions and shipping routes in the twenty-first century using CMIP6 forcing scenarios". In: *Environmental Research Letters* 15.10, p. 104079. DOI: 10.1088/1748-9326/abb2c8.

Wheeler, D. D., V. L. Harvey, D. E. Atkinson, R. L. Collins, and M. J. Mills (2011). "A climatology of cold air outbreaks over North America: WACCM and ERA-40 comparison and analysis". In: *Journal of Geophysical Research: Atmospheres* 116.D12. DOI: 10.1029/2011JD015711.

Wiel, K. van der, H. C. Bloomfield, R. W. Lee, L. P. Stoop, et al. (2019). "The influence of weather regimes on European renewable energy production and demand". In: *Environmental Research Letters* 14.9, p. 094010. DOI: 10.1088/1748-9326/ab38d3.

Woollings, T., D. Barriopedro, J. Methven, S.-W. Son, et al. (2018). "Blocking and its Response to Climate Change". In: *Current Climate Change Reports* 4.3, pp. 287–300. DOI: 10.1007/s40641-018-0108-z.

Woollings, T. and M. Blackburn (2012). "The North Atlantic Jet Stream under Climate Change and Its Relation to the NAO and EA Patterns". In: *Journal of Climate* 25.3, pp. 886–902. DOI: 10.1175/JCLI-D-11-00087.1.

Woollings, T., A. Hannachi, and B. Hoskins (2010). "Variability of the North Atlantic eddy-driven jet stream". In: *Quarterly Journal of the Royal Meteorological Society* 136.649, pp. 856–868. DOI: 10.1002/qj.625.

Wyser, K., T. Koenigk, U. Fladrich, R. Fuentes-Franco, et al. (2021). "The SMHI Large Ensemble (SMHI-LENS) with EC-Earth3.3.1". In: *Geoscientific Model Development* 14.7, pp. 4781–4796. DOI: 10.5194/gmd-14-4781-2021.

Yang, M., D. Luo, C. Li, Y. Yao, et al. (2021). "Influence of Atmospheric Blocking on Storm Track Activity Over the North Pacific During Boreal Winter". In: *Geophysical Research Letters* 48.17, e2021GL093863. DOI: 10.1029/2021GL093863.

Yiou, P., K. Goubanova, Z. X. Li, and M. Nogaj (2008). "Weather regime dependence of extreme value statistics for summer temperature and precipitation". In: *Nonlinear Processes in Geophysics* 15.3, pp. 365–378. DOI: 10.5194/npg-15-365-2008.

Yiou, P. and M. Nogaj (2004). "Extreme climatic events and weather regimes over the North Atlantic: When and where?" In: *Geophysical Research Letters* 31.7. DOI: 10.1029/2003GL019119.

Yu, H., J. A. Screen, S. Hay, J. L. Catto, and M. Xu (2023). "Winter Precipitation Responses to Projected Arctic Sea-Ice Loss and Global Ocean Warming and Their Opposing Influences over Northeast Atlantic region". In: *Journal of Climate* -1.aop, pp. 1–33. DOI: 10.1175/JCLI-D-22-0774.1.

Zappa, G., B. J. Hoskins, and T. G. Shepherd (2015). "The dependence of wintertime Mediterranean precipitation on the atmospheric circulation response to climate change". In: *Environmental Research Letters* 10.10, p. 104012. DOI: 10.1088/1748-9326/10/10/104012.

Zappa, G., L. C. Shaffrey, and K. I. Hodges (2013a). "The Ability of CMIP5 Models to Simulate North Atlantic Extratropical Cyclones". In: *Journal of Climate* 26.15, pp. 5379–5396. DOI: 10.1175/JCLI-D-12-00501.1.

Zappa, G., L. C. Shaffrey, K. I. Hodges, P. G. Sansom, and D. B. Stephenson (2013b). "A Multimodel Assessment of Future Projections of North Atlantic and European Extratropical Cyclones in the CMIP5 Climate Models". In: *Journal of Climate* 26.16, pp. 5846–5862. DOI: 10.1175/JCLI-D-12-00573.1.

Appendix

Methods

Pattern correlation coefficients

To compare two fields, area-weighted pattern correlation coefficients R_{pat} are calculated according to the following formula:

$$R_{pat} = \frac{Cov(a,b)}{\sqrt{Cov(a,a)\,Cov(b,b)}} \tag{1}$$

where the covariance $Cov(a,b)$ of two fields weighted by a vector of weights w is given by

$$Cov(a,b) = \frac{\sum_{i=1}^{N} w_i (X_{a,i} - \overline{X}_a)(X_{b,i} - \overline{X}_b)}{\sum_{i=1}^{N} w_i} \tag{2}$$

The weighted average $\overline{X}$ of the fields is obtained following:

$$\overline{X} = \frac{\sum_{i=1}^{N} X_i\, w_i}{\sum i = 1^N w_i} \tag{3}$$

In our case of area-weighted pattern correlation coefficients, the vector of weights w corresponds to the cosines of latitudes φ: $w = cos(\varphi)$.

To use this formula, the fields need to be flattened and the vector of weights needs to be adjusted accordingly. Then N corresponds to the number of latitudes times the number of longitudes.

Supplementary tables

Dataset	Explained variance
ERA5 Reanalysis	55.1%
Historical SMHI-LENS	53.1%
SSP5-8.5 scenario SMHI-LENS	52.2%

Table A1: Variance of the Z500 anomalies explained by the leading four EOFs in ERA5, the historical and the SSP5-8.5 simulation, respectively.

	NAO+	Scandinavian Blocking	Atlantic Ridge	NAO-
ERA5 and historical scenario	-0.071	0.933	0.697	0.651
Historical and SSP5-8.5 scenario	0.923	0.987	0.925	0.900

Table A2: Pattern correlation coefficients for the geopotential height anomalies associated with the different weather regimes identified in ERA5, the historical ensemble simulation and the future scenario simulation with the SMHI-LENS.
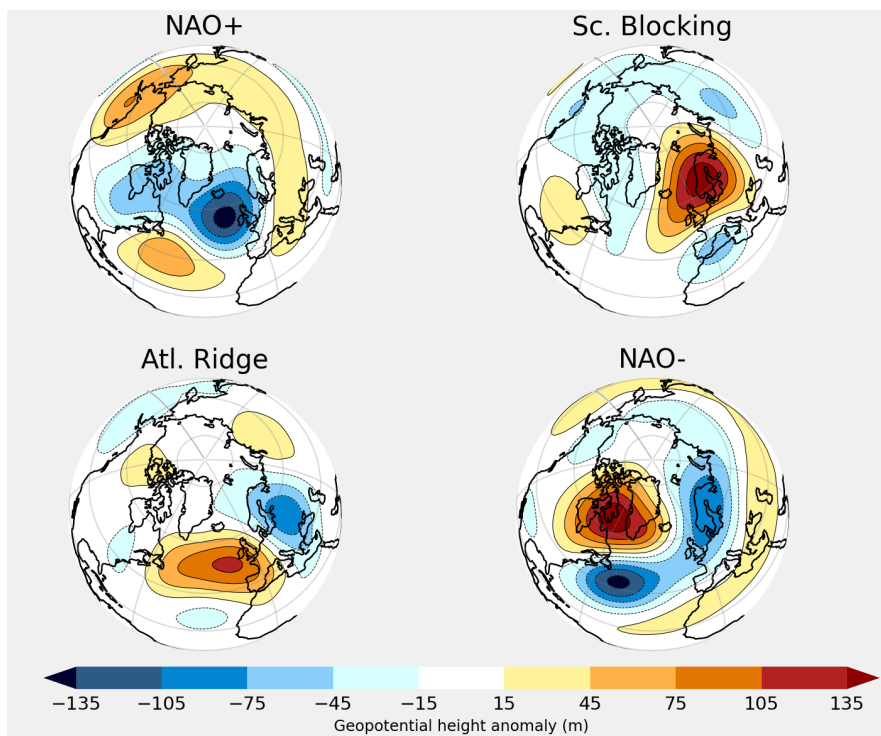
Supplementary figures

Figure A1: Composited geopotential height anomalies for the WRs identified using the leading 8 EOFs of Z500 anomalies in the ERA5 reanalysis data.
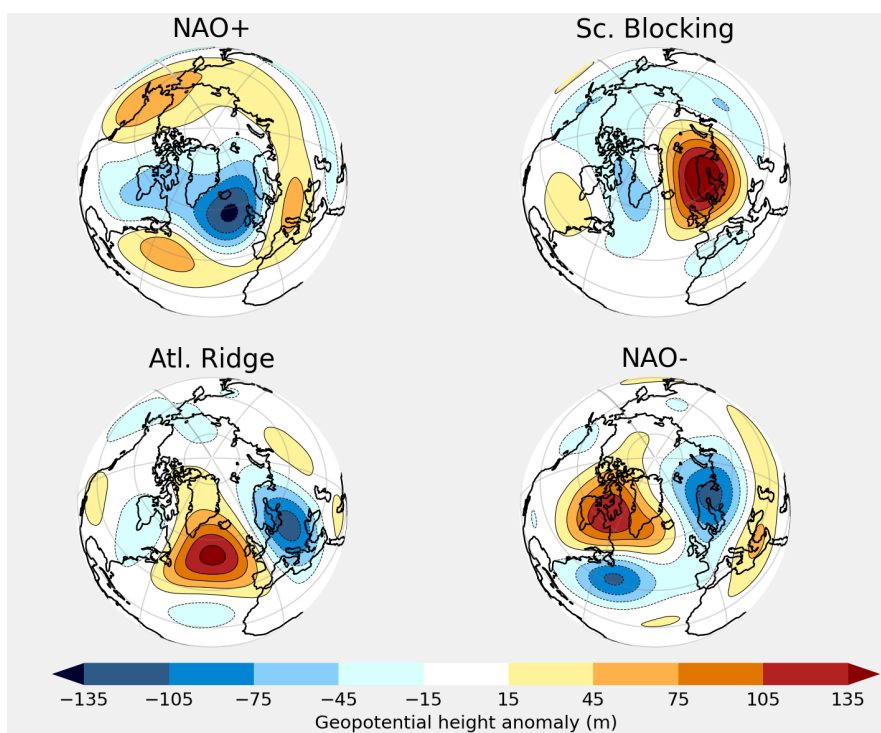

Figure A2: Weather regime composites as in Figure A1, but using the leading 10 EOFs.
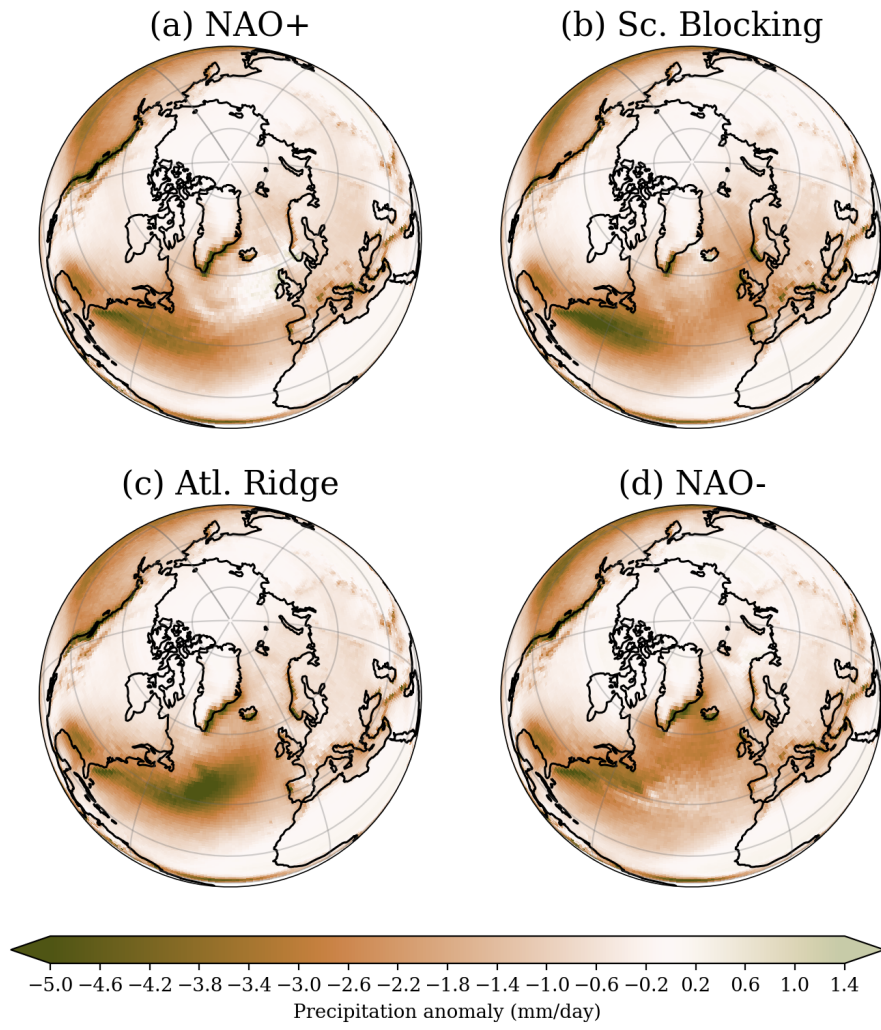
Figure A3: Composited median of total precipitation anomalies for the four WRs identified in ERA5 for the period 1979–2021.

Declaration

I confirm that the Master's thesis 'How will the dominant weather regimes change under the influence of climate warming?' is the result of my own work. No other person's work has been used without acknowledgement in the main text of this thesis. This thesis has not been submitted for the award of any other degree or thesis in any other institution. All sentences or passages quoted in this thesis from other people's work have been specifically acknowledged by clear cross-referencing to author, work and pages. Any illustrations which are not the work of the author of this thesis are specifically acknowledged. The submitted written version of the thesis corresponds to the version on the electronic storage device (filename: *Rahm_1104231.pdf*).

Date: ⎯⎯⎯⎯⎯⎯⎯⎯⎯⎯⎯⎯ Signature: ⎯⎯⎯⎯⎯⎯⎯⎯⎯⎯⎯⎯⎯⎯⎯⎯⎯⎯